The International Journal of Advanced Manufacturing Technology (2021) 114:423–449
https://doi.org/10.1007/s00170-021-06762-8

ORIGINAL ARTICLE

Multi-objective optimization of process parameters in plastic injection molding using a differential sensitivity fusion method

Huifang Zhou[1] · Shuyou Zhang[1] · Zili Wang[1]

Received: 16 October 2020 / Accepted: 2 February 2021 / Published online: 16 March 2021

Abstract

The product quality, productivity, and cost are mainly considered to make the manufacturing plan in plastic injection molding (PIM). The process parameters in PIM play a crucial role in determining the product quality, productivity, and cost. There are actually contradictions between above three properties. Therefore, it is difficult to quickly and accurately obtain the process parameters setting that meet the product quality requirement under the premise of acceptable productivity and cost. In this paper, a differential sensitivity fusion method (DSFM) is proposed to perform the multi-objective optimization of process parameters in PIM for the product quality and productivity improvement and the cost-saving, which integrates sampling strategy, numerical simulation, metamodeling method, and multi-objective optimization algorithm. The sampling strategy is utilized to generate sampling points from the design space at different parameter levels. For the sampling points, the numerical simulation is implemented to calculate the objective responses. Based on the sampling points and their corresponding response, the metamodeling method is applied to construct the response predictors to calculate the objective responses for any sampling point in the global design space. The multi-objective optimization algorithm is executed to locate the Pareto-optimal solutions, where the response predictors are taken as the fitness functions. The automobile front bumper is taken as the case study to verify the proposed method. The numerical results demonstrate that the proposed metamodeling method has better prediction accuracy and performance compared to some classical methods (e.g., response surface model, Kriging) and the multiple objectives cannot reach the optimal simultaneously. Moreover, the trade-off analysis identifies the better solution for decision-making, which helps to quickly and effectively select the optimal process parameters setting.

Keywords Plastic injection molding · Process parameters · Multi-objective optimization · DSFM · Trade-off analysis

1 Introduction

Plastic injection molding (PIM) is widely used to manufacture a wide variety of plastic products owing to its high productivity, low cost, and good flexibility to various complex geometries. PIM is a nonlinear coupled system with multiple inputs and multiple outputs. The output includes product quality, manufacturing cost, and molding efficiency, whereas the input includes machine characteristics, mold design pattern, process parameters, polymer material characteristics, and product geometric characteristics. The machine, mold, material, and product will determined before manufacturing, which means that the process parameters should be carefully set to avoid or reduce quality defects, improve productivity, and decrease energy consumption and cost.

To reduce the product defects (e.g., warpage, shrinkage, weldline), processing conditions, material properties, product design, and mold design have been studies by many researchers. Ozcelik and Sonat [1] used the Taguchi method to study the effect of process parameters on the warpage of parts with different thicknesses. Oktem et al. [2] conducted a series of experiments and used the signal-to-noise (S/N) ratio method and analysis of variance (ANOVA) to study the effects of process parameters on warpage and shrinkage of products. Tang et al. [3] performed warpage experiments on a thin plate to study the impact factors of the warpage problem. Kurt et al. [4] investigated the influence of the cavity pressure and mold surface temperature on the quality of the final parts. Masato

✉ Zili Wang
ziliwang@zju.edu.cn

[1] State Key Laboratory of Fluid Power and Mechatronic Systems, Zhejiang University, Hangzhou 310027, People's Republic of China

et al. [5] analyzed and concluded that the shrinkage for thin-wall parts was caused by fiber orientation and could be reduced by higher melt temperature, packing pressure. Wang et al. [6] investigated the structural carbon emissions and injection molding process carbon emissions and implemented multi-objective optimization to realize the low-carbon design for injection molding machine.

Different from the constant process parameter optimization, the variable process parameter profile (e.g., packing pressure profile) has been considered to improve product quality and efficiency. Li et al. [7] performed the optimization of variable packing pressure profile for the shrinkage evenness of a slab. Gao and Wang [8] applied the sequential approximate optimization (SAO) to determine the optimal packing profile and the optimal process parameters for warpage minimization. For minimizing warpage and cycle time, Kitayama et al. [9] investigated the multi-objective optimization of variable pressure profile and process parameters. Hashimoto et al. [10] applied SAO to realize the simultaneous optimization of variable injection velocity profile and process parameters for minimizing weldline and cycle time.

Due to the advance of computer technology, computer-aided simulation software (e.g., Moldflow, Moldex3D) coupled with design optimization is recognized as an alternative approach for determining the optimal process parameters. The numerical simulation in PIM is generally so intensive that the surrogate-based or metamodeling approach, which can establish a mathematical relationship between the process parameters and optimization objectives, is valid to determine the optimal process parameters with a small number of simulations. Ozcelik and Erzurumlu [11] integrated finite element analysis (FEA), statistical DOE methods, RSM, and genetic algorithm (GA) to minimize the warpage of thin-walled parts. Kurtaran et al. [12] integrated the FEA, statistical DOE methods, ANN, and GA to minimize the warpage of automotive ceiling lamps. Gao and Wang [13] adopted the Kriging model for determining the optimal process parameters to minimize the warpage of a cellular phone cover. Li et al. [7] used the radial basis function (RBF) and the expected improvement (EI) to optimize the process parameters for achieving uniform shrinkage. Xia et al. [14] adopted the Gaussian process (GP) model for the front grille's warpage optimization. The above researches handle a single objective optimization, but there are generally many objectives to optimization for high product quality and productivity in PIM. Chen and Kumiawan [15] proposed a two-stage multi-objective optimization system. Zhao et al. [16] proposed a two-stage optimization system to optimize the warpage, shrinkage, and sink marks of injection molded parts simultaneously. Zhao and Cheng [17] proposed a hybrid multi-objective optimization system to simultaneously optimize the warpage and cycle time of the PIM process. Cheng et al. [18] developed a novel method to find the optimal solution set of constrained multi-objective optimization problems that integrated variable complexity methods (VCMs), constrained non-dominated sorting genetic algorithm (CNSGA), BPNN, and Moldflow analysis. Liu et al. [19] proposed a multi-objective optimization method for process parameters of PIM with the haze ratio (HR) and peak valley 20 (PV20) of an optical lens as the optimization target. Xu et al. [20, 21] performed the process parameter optimization for minimizing the weight, the flash, and the volume shrinkage of a thin-walled plastic product.

In particular, a sequential approximate optimization (SAO) that the surrogate model is repeatedly constructed and optimized by adding several new sampling points has gradually been a popular approach to improve the optimization result. The general framework of the process parameters optimization in PIM using the SAO is summarized in [22]. Several representative papers using SAO approach is briefly reviewed. Gao and Wang [8, 13] adopted the modified rectangular grid (MRG) sampling strategy and the expected improvement (EI) sampling criterion to improve the accuracy of the Kriging model, respectively. Xia et al. [14] used an enhanced probability of improvement criterion to find the direction of adding training samples and optimize the surrogate model. Shi et al. [23] used a parametric sampling evaluation (PSE) strategy to improve the accuracy of the ANN model and speed up the optimization process to converge to the global optimum. Deng et al. [24] used the mode-pursuing sampling strategy (MPS) to obtain new sample points, thereby improving the accuracy of the Kriging model.

In addition to the optimization of process parameters, the conformal cooling channel is applied to improve the product quality and efficiency of PIM. Dimla et al. [25] reported that the conformal cooling channel could drastically reduce cycle time. Au and Yu [26] designed various scaffold cooling channels and evaluated the cooling performance and found that the conformal cooling channel could offer a more uniform thermal distribution. Wang et al. [27] introduced an approach to generate conformal spiral cooling channels, which helped improve the uniform of mold cooling. Kitayama et al. [10, 28–30] investigated the cooling performance of the conventional straight-type cooling channels and conformal cooling channels numerically and experimentally where the process parameter optimization for warpage, cycle time, weldline, and clamping force reduction was performed.

Here, the motivation for this paper is summarized as follows:

1. Multi-objective optimization of process parameters in PIM is a crucial issue. Several process parameters are optimized for warpage and weldline reduction, and clamping force and cycle time minimization.
2. Weldlines are one of the major defects, which cannot be completely eliminated. The low weldline temperature

generates long weldlines for the quick solidification. The minimum weldline temperature is considered to be maximized for weldline reduction.

3. The sensitivity information of sampling points is used to improve the prediction accuracy of the response predictor. Therefore, the performance of multi-objective optimization can be improved.
4. In general, warpage, weldline, clamping force, and cycle time cannot reach the optimal at the same time. Therefore, the trade-off analysis is implemented to make the decision for the multi-objective optimization.

To realize the high product quality, high productivity, and low energy consumption and cost in PIM, this paper proposes a differential sensitivity fusion method (DSFM) to perform the multi-objective optimization of process parameters in PIM for minimizing warpage, weldlines, clamping force, and cycle time. It integrates the sampling strategy, numerical simulation, metamodeling method, and multi-objective optimization algorithm. The sampling strategy, Latin hypercube sampling (LHS), is utilized to generate stratified and uniformly distributed sampling points from the design space. For sampling points, the numerical simulation based on Moldflow is implemented to calculate the responses. Based on the sampling points and their corresponding responses, the metamodeling method is applied to construct the response predictors to calculate the responses for any sampling point in the global design space. The gradient-enhanced response surface model (GERSM) combined with the moving least-squares method (MLSM) is applied to construct the response predictor for each objective, which simultaneously utilizes the response and sensitivity information of the sampling point to improve the accuracy of the response predictors. For the capture of the sensitivity information, an adaptive sensitivity generation method (ASGM) is proposed to calculate the gradient vector for each design variable of the sampling point. The multi-objective optimization algorithm, non-dominated sorting genetic algorithm-III (NSGA-III), is executed to locate the Pareto-optimal solutions, where the response predictors are taken as the fitness functions. The trade-off analysis based on the spider-web chart is applied to make the decision for the optimal process parameters. Moreover, for the structural features of the product, the valve hot runner system is applied to reduce the weldlines and improve the product surface quality. The automobile front bumper is taken as a case study to verify the proposed method DSFM. The numerical results show that the proposed method can help the manufacturers to quickly and accurately select the optimal process parameters setting.

The remainder of the rest of this paper is organized as follows. In Section 2, the multi-objective optimization problem and the trade-off analysis based on the spider-web chart are described. In Section 3, the optimization methodologies and the detailed process for realizing the multi-objective optimization of the process parameters in PIM are described. To verify the proposed method, the automobile front bumper is taken as the case study and the numerical results are shown in Section 4. Finally, the conclusion is drawn in Section 5.

2 Overview of multi-objective optimization problem

2.1 Multi-objective optimization model

The goal of the injection molding process parameters (IMPP) optimization is to improve the product quality and productivity, while reducing cost. It is a typical multi-objective optimization problem. A multi-objective design optimization problem can be generally formulated as follows:

$$\begin{aligned} &\text{find}: \boldsymbol{x} = [x_1, x_2, \cdots, x_D]^T, \\ &\text{minimize} F(\boldsymbol{x}) = \text{minimize}(f_1(\boldsymbol{x}), f_2(\boldsymbol{x}), \cdots, f_K(\boldsymbol{x})), \\ &\text{Subject to}: \\ &x_i^L \le x_i \le x_i^H, \quad i = 1, 2, \cdots, D \end{aligned} \tag{1}$$

where $\boldsymbol{x}$ is the column vector of the design variables, and $x_i (i = 1, 2, \cdots, D)$ represents the i-th deign variable; D is the number of the design variables; $f_j(\boldsymbol{x})$ $(j = 1, 2, \cdots, K)$ is the j-th objective function to be minimized, and K is the number of the objective functions; x_i^L and x_i^H are the lower and upper bounds of the i-th design variable, respectively.

2.2 Objective functions

Warpage is one of the major defects in PIM. It causes the actual dimensions of the product to deviate from the design requirement, which should be minimized for high product quality. The first objective function $f_1(\boldsymbol{x})$ is taken as the warpage.

Weldlines influence the appearance of the product and the product strength. It is significant to reduce the weldlines of the product. The weldline will generate when two or more flow fronts meet. The melted plastic will be quickly solidified with the low weldline temperature, which causes the generation of long weldlines. The weldline temperature is one of the important factors for the weldline reduction [29, 30]. The minimum weldline temperature ($MinT_{\text{weld}}$) needs to be maximized for weldline reduction. Therefore, the opposite of the minimum weldline temperature is taken as the second objective function $f_2(\boldsymbol{x})$, and is minimized.

Energy consumption and cost is also an important issue in PIM. When the melted plastic is injected into the cavity, a reversed pressure will generate. The clamping force should be applied to keep the mold closed. Small clamping force

can reduce the energy consumption and save the cost. Therefore, clamping force is taken as the third objective function $f_3(\boldsymbol{x})$ for energy consumption reduction.

Cycle time directly influences the molding efficiency and should be minimized for high productivity, so it is taken as the fourth objective function $f_4(\boldsymbol{x})$. The sum of the injection time, the packing time, and the cooling time can be evaluated as the cycle time, which is expressed as:

$$f_4(\boldsymbol{x}) = t_{inj} + t_p + t_c, \tag{2}$$

where t_{inj} is the injection time; t_p is the packing time; t_c is the cooling time.

2.3 Design variables

The melt temperature (T_{melt}), the mold temperature (T_{mold}), the injection time (t_{inj}), the packing pressure, the packing time, and the cooling time (t_c) are taken as the design variables. To ensure the improvement of the products dimensional accuracy and the consistency of the product shrinkage degree, a variable packing pressure profile instead of constant packing pressure is applied, as shown in Fig. 1.

The packing pressure profile consists four parameters (packing pressure P_{p1}, P_{p2} and packing time t_{p1}, t_{p2} at point A and B in Fig. 1). Therefore, the design variables are $\boldsymbol{x} = [T_{\text{melt}}, T_{\text{mold}}, t_{inj}, P_{p1}, P_{p2}, t_{p1}, t_{p2}, t_c]^T$. The lower and upper bound of design variables are shown in Table 1, which are determined by the recommended values in Moldflow and the manufacture's recommendation.

2.4 Trade-off analysis

For the multi-objective optimization problem expressed in Eq. (1), we want to minimize all the objectives simultaneously. Because of the contradiction between the objectives and their possible incommensurability, it is impossible to find a solution to ensure that all the objectives are simultaneously optimal. Thus, there is no single optimal solution but rather a set of compromise solutions named Pareto-optimal solutions or non-dominated solutions to such an optimization problem with multiple conflicting objectives.

After the Pareto-optimal solution set has been generated, the decision-maker should perform the trade-off analysis to select the most preferred one or a few solutions among the alternatives for producing the product. The spider-web chart or radar chart can visually understand the trade-off over three objectives, and is one of the useful tools for the trade-off analysis [31]. An illustrative example of a spider-web chart for the Pareto-optimal solutions visualization is shown in Fig. 2, in which four objective functions to be minimized is handled. Each apex of a polygon in Fig. 2 represents one objective. The outermost polygon shows the nadir solution, the innermost polygon represents the ideal solution, and the middle polygons present the alternatives.

Because of the difference of value range between the objectives, each apex is normalized using Eq. (3) to draw the spider-web chart.

$$\overline{f_j}\left(\boldsymbol{x}_p^{(i)}\right) = \frac{f_j\left(\boldsymbol{x}_p^{(i)}\right) - f_j^I}{f_j^N - f_j^I} \quad i = 1, 2, \cdots, \tag{3}$$

$$N_{alt} \quad j = 1, 2, \cdots, K$$

where $\boldsymbol{x}_p^{(i)}$ denotes the i-th alternative (Pareto-optimal solution); N_{alt} is the number of the Pareto-optimal solutions; $f_j\left(\boldsymbol{x}_p^{(i)}\right)$ and $\overline{f_j}\left(\boldsymbol{x}_p^{(i)}\right)$ represent the unnormalized and normalized value of the j-th objective of $\boldsymbol{x}_p^{(i)}$, respectively; K is the number of the objectives; f_j^I and f_j^N denote the ideal and nadir value of the j-th objective.

The area of each polygon in the spider-web chart is used to compare the alternatives. The Pareto-optimal solutions minimizing and maximizing the polygon area in the spider-web chart are taken as the better solution and the worse solution, respectively.

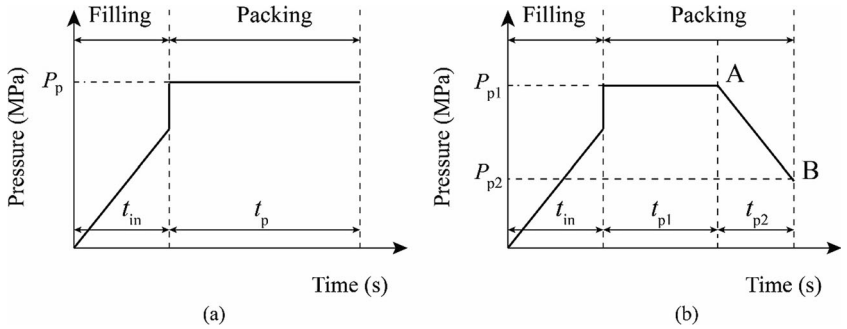

Fig. 1 Packing pressure profiles. **a** Constant packing pressure profile; **b** variable packing pressure profile

Table 1 Design variables and their lower/upper bounds

Design variable	Lower bound	Upper bound
Melt temperature T_{melt} [°C]	230	250
Mold temperature T_{mold} [°C]	40	80
Injection time t_{inj} [s]	3	8
Packing pressure P_{p1} [MPa]	100	110
Packing pressure P_{p2} [MPa]	40	70
Packing time t_{p1} [s]	20	25
Packing time t_{p2} [s]	35	40
Cooling time t_c [s]	20	40

3 Optimization methodologies

3.1 Multi-objective optimization process

The method, DSFM, is proposed to realize the process parameter optimization in PIM for warpage and weldlines reduction and clamping force and cycle time minimization, which integrates the sampling strategy, numerical simulation, metamodeling method, and multi-objective optimization algorithm. The sampling strategy is utilized to generate sampling points from the design space at different parameter levels. For the sampling points, the numerical simulation based on Moldflow is implemented to calculate the responses (warpage, minimum weldline temperature, clamping force, and cycle time). Based on the sampling points and their corresponding response, the metamodeling method is applied to approximately represent the mathematical relationship between the design variables (process parameters) and the responses, which constructs the response predictors to calculate the responses for any sampling point in the global design space. The multi-objective optimization algorithm, NSGA-III, is executed to locate the Pareto-optimal solutions, where the response predictors are taken as the fitness functions. The flowchart of our proposed method to realize multi-objective process parameter optimization in PIM is shown in Fig. 3.

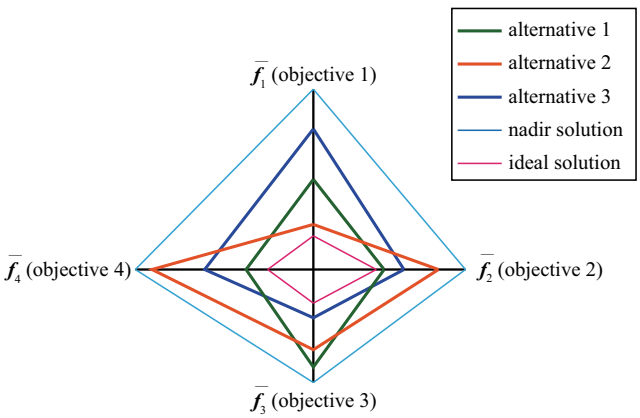

Fig. 2 An illustrative example of spider-web chart including four objectives

As shown in Fig. 3, the main steps of the proposed method include the acquisition and processing of the sampling points, the response predictor modeling, and the multi-objective optimization. The specific process can be described as:

Step 1: Identify the responses as the objectives and the process parameters related to the selected responses as the design variables of the optimization problem. Determine the value range of each design variable as the constraints of the optimization problem.
Step 2: Implement the sampling strategy, LHS, to generate stratified, and uniformly distributed sampling points in the global design space, and execute the numerical simulation to calculate and obtain the responses for each sampling point based on the Moldflow.
Step 3: Apply the sensitivity analysis among the design variables and the responses to identify the most important design variables that have a significant influence on the selected objectives.
Step 4: Response predictor modeling based on the metamodeling method. Taking the sampling points obtained in Step 2 as the training set (displayed in Table 11 ~ 12 in Appendix), the proposed method, ASGM, is implemented to calculate the gradient vector for each design variable of each sampling point in the training set as the sensitivity information of the training set. Then, based on the response and sensitivity information of the sampling points, the GERSM combined with the MLSM is constructed as the response predictor for each selected objective.
Step 5: Multi-objective process parameter optimization based on NSGA-III algorithm. Set the initial parameters of NSGA-III algorithm, and then take the response predictors constructed in Step 4 as the fitness functions to perform multi-objective global optimization and locate the Pareto-optimal solution set. For the Pareto-optimal solutions, the trade-off analysis is implemented to locate a better solution.
Step 6: Organize the confirmation experiments (as shown in Table 13 ~ 14 in Appendix) to verify the effectiveness of the proposed method.

3.2 Response predictor modeling

3.2.1 GERSM metamodeling

Compared with the traditional response surface model (RSM), the GERSM utilizes not only the response information but

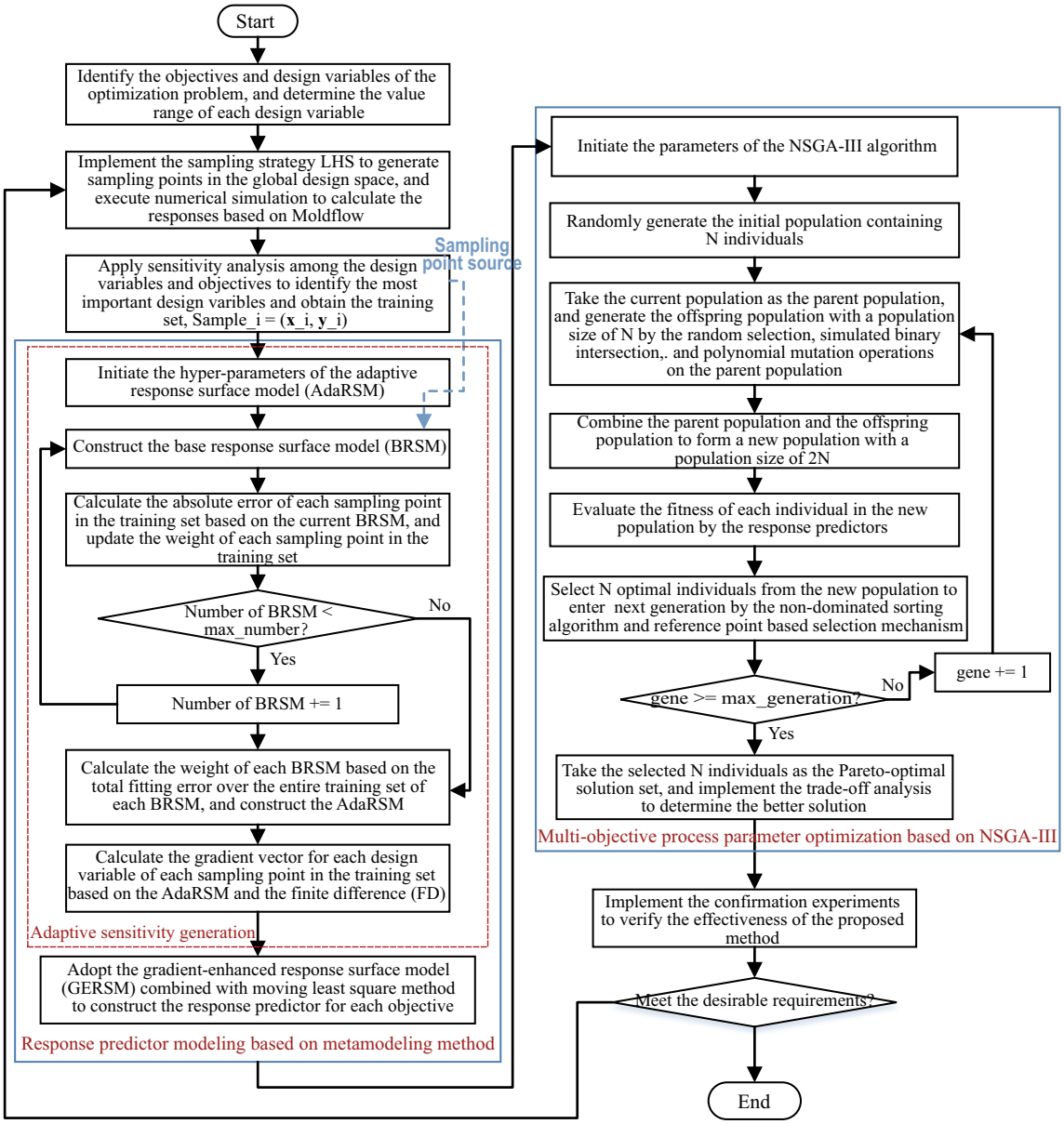

Fig. 3 Flowchart of the proposed method

also the sensitivity information of the sampling points to construct the response surface [32]. The total error consists of response error and gradient error. In addition, the MLSM is a local approximation method, which is essentially a weighted least-squares method, and it uses weighting factors and local approximation to improve the accuracy of least-squares fitting when constructing a surrogate model [33].

Combined with the MLSM, the surface was constructed by GERSM changes with the position of the point in the design space. Therefore, the total error and regression coefficients are functions of the sampling point position, which can be defined as:

$$\boldsymbol{\beta}(\boldsymbol{x}) = \arg\min_{\boldsymbol{\beta}} E_{\text{total}}(\boldsymbol{x}) = \arg\min_{\boldsymbol{\beta}} \left[(1-\text{swg}) \cdot E_y(\boldsymbol{x}) + \text{swg} \cdot E_g(\boldsymbol{x})\right] \quad (4)$$

$$\boldsymbol{x} = [x_1, x_2, \cdots, x_D]^{\mathrm{T}} \in \mathbb{R}^D \quad (5)$$

where $\boldsymbol{\beta}(\boldsymbol{x})$ is the regression coefficient vector; $E_{\text{total}}(\boldsymbol{x})$ is the total error function; $\boldsymbol{x}$ is the general sampling point; D is the number of the design variables; $\mathbb{R}^D$ is the design space; swg is the sensitivity control factor for measuring the effect of the response information and the gradient information on the total fitting error; $E_y(\boldsymbol{x})$ and $E_g(\boldsymbol{x})$ represent the response error function and the gradient error function, respectively.

The second order polynomial is used to construct the response surface, which can be defined as:

$$\widehat{y}(\boldsymbol{x}) = b_0 + \sum_{i=1}^{D} b_i \cdot x_i + \sum_{i=1}^{D} b_{ii} \cdot {x_i}^2 + \sum_{i=1}^{D} \sum_{j>i}^{D} b_{ij} \cdot x_i x_j \tag{6}$$

where $\widehat{y}(\boldsymbol{x})$ is the response surface; mapping b_0, b_i, b_{ii}, b_{ij}: $\boldsymbol{x} \to \mathbb{R}$ project sampling point to its corresponding regression coefficients; x_i and x_j denote the i-th and j-th design variable, respectively.

According to Eq. (6), the error function $E_y(\boldsymbol{x})$ and $E_g(\boldsymbol{x})$ are formulated as follows:

$$E_y(\boldsymbol{x}) = (\boldsymbol{y} - \mathbf{X}\cdot\boldsymbol{\beta}(\boldsymbol{x}))^{\mathrm{T}} \mathbf{W}_y(\boldsymbol{x}) (\boldsymbol{y} - \mathbf{X}\cdot\boldsymbol{\beta}(\boldsymbol{x})) \tag{7}$$

$$E_g(\boldsymbol{x}) = \sum_{i=1}^{D} \left(\boldsymbol{g}_{x_i} - \mathbf{T}_{x_i}\cdot\boldsymbol{\beta}(\boldsymbol{x})\right)^{\mathrm{T}} \mathbf{W}_g(\boldsymbol{x}) \left(\boldsymbol{g}_{x_i} - \mathbf{T}_{x_i}\cdot\boldsymbol{\beta}(\boldsymbol{x})\right) \tag{8}$$

where $\boldsymbol{y}$ is the true response vector; $\boldsymbol{g}_{x_i}$ is the true gradient vector for the i-th design variable of $\boldsymbol{x}$; $\mathbf{X}$ denotes the response design matrix; $\mathbf{T}_{x_i}$ denotes the response and gradient design matrix of the i-th design variable, which is the partial derivative of $\mathbf{X}$ to the i-th design variable; the diagonal matrices $\mathbf{W}_y(\boldsymbol{x})$ and $\mathbf{W}_g(\boldsymbol{x})$ represent the response and gradient weight matrix, respectively.

The vector $\boldsymbol{y}$ and $\boldsymbol{\beta}(\boldsymbol{x})$, the matrices $\mathbf{X}$, $\mathbf{T}_{x_i}$, $\mathbf{W}_y(\boldsymbol{x})$ and $\mathbf{W}_g(\boldsymbol{x})$ can be formulated as follows:

$$\boldsymbol{y} = \begin{bmatrix} y^{(1)} & y^{(2)} & \cdots & y^{(k)} & \cdots & y^{(N)} \end{bmatrix}^{\mathrm{T}} \tag{9}$$

$$\boldsymbol{\beta}(\boldsymbol{x}) = \begin{bmatrix} b_0 & b_1 & \cdots & b_i & \cdots & b_D & b_{11} & \cdots & b_{ii} & \cdots & b_{ij} & \cdots & b_{(D-1)D} \end{bmatrix}^{\mathrm{T}} \tag{10}$$

$$\mathbf{X} = \begin{bmatrix} 1 & x_1^{(1)} & \cdots & x_i^{(1)} & \cdots & x_D^{(1)} & {x_1^{(1)}}^2 & \cdots & {x_i^{(1)}}^2 & \cdots & x_i^{(1)} x_j^{(1)} & \cdots & x_{D-1}^{(1)} x_D^{(1)} \\ \vdots & \vdots & \ddots & \vdots & \ddots & \vdots & \vdots & \ddots & \vdots & \ddots & \vdots & \ddots & \vdots \\ 1 & x_1^{(k)} & \cdots & x_i^{(k)} & \cdots & x_D^{(k)} & {x_1^{(k)}}^2 & \cdots & {x_i^{(k)}}^2 & \cdots & x_i^{(k)} x_j^{(k)} & \cdots & x_{D-1}^{(k)} x_D^{(k)} \\ \vdots & \vdots & \ddots & \vdots & \ddots & \vdots & \vdots & \ddots & \vdots & \ddots & \vdots & \ddots & \vdots \\ 1 & x_1^{(N)} & \cdots & x_i^{(N)} & \cdots & x_D^{(N)} & {x_1^{(N)}}^2 & \cdots & {x_i^{(N)}}^2 & \cdots & x_i^{(N)} x_j^{(N)} & \cdots & x_{D-1}^{(N)} x_D^{(N)} \end{bmatrix} \tag{11}$$

$$\mathbf{T}_{x_i} = \begin{bmatrix} 0 & 0 & \cdots & 1 & \cdots & 0 & 0 & \cdots & 2x_i^{(1)} & \cdots & x_j^{(1)} & \cdots & 0 \\ \vdots & \vdots & \ddots & \vdots & \ddots & \vdots & \vdots & \ddots & \vdots & \ddots & \vdots & \ddots & \vdots \\ 0 & 0 & \cdots & 1 & \cdots & 0 & 0 & \cdots & 2x_i^{(k)} & \cdots & x_j^{(k)} & \cdots & 0 \\ \vdots & \vdots & \ddots & \vdots & \ddots & \vdots & \vdots & \ddots & \vdots & \ddots & \vdots & \ddots & \vdots \\ 0 & 0 & \cdots & 1 & \cdots & 0 & 0 & \cdots & 2\mathrm{x}_i^{(k)} & \cdots & x_j^{(N)} & \cdots & 0 \end{bmatrix} \tag{12}$$

$$\mathbf{W}_y(\boldsymbol{x}) = \begin{bmatrix} \omega_y\left(\boldsymbol{x} - \boldsymbol{x}^{(1)}\right) & \cdots & 0 & \cdots & 0 \\ \vdots & \ddots & \vdots & \vdots & \vdots \\ 0 & \cdots & \omega_y\left(\boldsymbol{x} - \boldsymbol{x}^{(k)}\right) & \cdots & 0 \\ \vdots & \vdots & \vdots & \ddots & \vdots \\ 0 & \cdots & 0 & \cdots & \omega_y\left(\boldsymbol{x} - \boldsymbol{x}^{(N)}\right) \end{bmatrix} \tag{13}$$

$$\mathbf{W}_g(\boldsymbol{x}) = \begin{bmatrix} \omega_g\left(\boldsymbol{x} - \boldsymbol{x}^{(1)}\right) & \cdots & 0 & \cdots & 0 \\ \vdots & \ddots & \vdots & \vdots & \vdots \\ 0 & \cdots & \omega_g\left(\boldsymbol{x} - \boldsymbol{x}^{(k)}\right) & \cdots & 0 \\ \vdots & \vdots & \vdots & \ddots & \vdots \\ 0 & \cdots & 0 & \cdots & \omega_g\left(\boldsymbol{x} - \boldsymbol{x}^{(N)}\right) \end{bmatrix} \tag{14}$$

where $y^{(k)}$ denotes the true response of the k-th sampling point; N is the size of the sampling points; $\boldsymbol{x}^{(k)}$ denotes the k-th sampling point; $x_i^{(k)}$ denotes the i-th design variable of the k-th sampling point. The element $\omega_y(\boldsymbol{x} - \boldsymbol{x}^{(k)})$ and $\omega_g(\boldsymbol{x} - \boldsymbol{x}^{(k)})$ on the diagonal denote the weight of $\boldsymbol{x}^{(k)}$ for the calculation of response and gradient error, respectively. The exponential function is applied as the weight function to calculate $\omega_y(\boldsymbol{x} - \boldsymbol{x}^{(k)})$ and $\omega_g(\boldsymbol{x} - \boldsymbol{x}^{(k)})$. The formulas are as follows:

$$\omega_y\left(\boldsymbol{x} - \boldsymbol{x}^{(k)}\right) = \omega_g\left(\boldsymbol{x} - \boldsymbol{x}^{(k)}\right) = \omega(d) = \begin{cases} \exp\left(-\dfrac{d}{\mathrm{RI}}\right), & \dfrac{d}{\mathrm{RI}} \le 1 \\ 0, & \dfrac{d}{\mathrm{RI}} > 1 \end{cases} \tag{15}$$

$$d = \left\|\boldsymbol{x} - \boldsymbol{x}^{k}\right\|_2 = \left[\sum_{i=1}^{D} \left(x_i - x_i^{(k)}\right)^2\right]^{1/2} \tag{16}$$

where $\omega_y(\cdot)$ and $\omega_g(\cdot)$ denote the response and gradient weight function, respectively; RI is the size of the support region, which means that only the sampling point located in the support region will have an impact on the prediction of $\boldsymbol{x}$; d is the Euclidean distance between $\boldsymbol{x}$ and $\boldsymbol{x}^{(k)}$.

According to the Eq. (4), the regression coefficient vector $\boldsymbol{\beta}(\boldsymbol{x})$ of GERSM can be obtained by the following set of equations:

$$\frac{\partial E_{\text{total}}(\boldsymbol{x})}{\partial \boldsymbol{\beta}} = (1-\text{swg}) \cdot \frac{\partial E_y(\boldsymbol{x})}{\partial \boldsymbol{\beta}} + \text{swg} \cdot \frac{\partial E_g(\boldsymbol{x})}{\partial \boldsymbol{\beta}} = 0 \tag{17}$$

$$\boldsymbol{\beta}(\boldsymbol{x}) = A(\boldsymbol{x})^{-1} B(\boldsymbol{x}) \tag{18}$$

$$A(\boldsymbol{x}) = (1-\text{swg}) \cdot \mathbf{X}^{\mathrm{T}} \mathbf{W}_y(\boldsymbol{x}) \mathbf{X} + \text{swg} \cdot \sum_{i=1}^{D} \mathbf{T}_{x_i}{}^{\mathrm{T}} \mathbf{W}_g(\boldsymbol{x}) \mathbf{T}_{x_i} \tag{19}$$

$$B(\boldsymbol{x}) = (1-\text{swg}) \cdot \mathbf{X}^{\mathrm{T}} \mathbf{W}_y(\boldsymbol{x}) \boldsymbol{y} + \text{swg} \cdot \sum_{i=1}^{D} \mathbf{T}_{x_i}{}^{\mathrm{T}} \mathbf{W}_g(\boldsymbol{x}) \boldsymbol{g}_{x_i} \tag{20}$$

Base on the GERSM, the response of $\boldsymbol{x}$ can be predicted as:

$$\widetilde{y} = (1-\text{swg}) \cdot \boldsymbol{x}^p \boldsymbol{\beta}(\boldsymbol{x}) + \text{swg} \cdot \sum_{i=1}^{D} \boldsymbol{t}_{x_i} \boldsymbol{\beta}(\boldsymbol{x}) \tag{21}$$

$$\boldsymbol{x}^p = \begin{bmatrix} 1 & x_1 & \cdots & x_i & \cdots & x_D & {x_1}^2 & \cdots & {x_i}^2 & \cdots & x_i x_j & \cdots \end{bmatrix} \tag{22}$$

$$\boldsymbol{t}_{x_i} = \begin{bmatrix} 0 & 0 & \cdots & 1 & \cdots & 0 & 0 & \cdots & 2x_i & \cdots & x_j & \cdots & 0 \end{bmatrix} \tag{23}$$

where $\boldsymbol{x}^p$ denotes the response design vector of $\boldsymbol{x}$; $\boldsymbol{t}_{x_i}$ denotes the gradient design vector for the i-th design variable of $\boldsymbol{x}$.

3.2.2 Adaptive sensitivity generating

The construction of the GERSM simultaneously requires the response and sensitivity information of the sampling points. Through numerical or practical experiment, only the response information can be obtained. Therefore, based on the finite difference (FD), ASGM is proposed to obtain the sensitivity information of the sampling points. For the general sampling point $\boldsymbol{x}$ in the design space, the general process of capturing the sensitivity information of $\boldsymbol{x}$ is as follows: Firstly, an adaptive response surface model (AdaRSM) is constructed as the strong predictor, which is proposed to explore the compact neighborhood of $\boldsymbol{x}$. Then, the response of the new sampling point in the compact neighborhood of $\boldsymbol{x}$ can be given by the strong predictor AdaRSM. Finally, the FD is used to calculate the gradient vector of $\boldsymbol{x}$.

The AdaRSM is the linear combination of a series of base response surface model (BRSM), which are generate by iteratively updating the weights of the sampling points. The AdaRSM can be expressed as:

$$\widehat{\boldsymbol{f}}(\boldsymbol{x}) = \sum_{m=1}^{M} \alpha^{(m)} \cdot \text{RSM}^{(m)}(\boldsymbol{x}) \tag{24}$$

where $\widehat{\boldsymbol{f}}(\boldsymbol{x})$ is the adaptive response surface; $\alpha^{(m)}$ denotes the weight of the m-th BRSM; $RSM^{(m)}(\boldsymbol{x})$ is the m-th BRSM; $\boldsymbol{x}$ is the general sampling point, as shown in Eq. (5); M is the number of the BRSM.

The construction of AdaRSM includes the following steps: (1) initialize the weights of the sampling points and constructing the BRSM; (2) calculate the total error of the BRSM over the entire samples; (3) update the weight of each sampling point according to the prediction error of the BRSM for each sampling point; (4) iteratively construct the next BRSM based on the updated weights of the sampling points. Repeat steps (2)-(4) until the target number of the BRSM has been reached. (5) Calculate the weight of each BRSM according to the total error of each BRSM. The m-th BRSM can be expressed as:

$$\text{RSM}^{(m)}(\boldsymbol{x}) = a_0^{(m)} + \sum_{i=1}^{D} a_i^{(m)} \cdot x_i + \sum_{i=1}^{D} a_{ii}^{(m)} \cdot x_i^2 + \sum_{i=1}^{D} \sum_{j>i}^{D} a_{ij}^{(m)} \cdot x_i x_j = \boldsymbol{x}^p \boldsymbol{\beta}^{(m)} \tag{25}$$

$$\boldsymbol{\beta}^{(m)} = \left(\mathbf{X}^{\mathrm{T}} \mathbf{W}^{(m)} \mathbf{X}\right)^{-1} \mathbf{X}^{\mathrm{T}} \mathbf{W}^{(m)} \boldsymbol{y} \tag{26}$$

where $a_0^{(m)}$, $a_i^{(m)}$, $a_{ii}^{(m)}$, and $a_{ij}^{(m)}$ are the regression coefficients of the m-th BRSM; $\boldsymbol{\beta}^{(m)}$ denotes the regression coefficient vector of the m-th BRSM; $\boldsymbol{x}^p$, $\mathbf{X}$, and $\boldsymbol{y}$ are as shown in Eq. (22), (11), and (9); $\mathbf{W}^{(m)}$ represents the weight matrix of the sampling points when constructing the m-th BRSM, which can be formulated as:

$$\mathbf{W}^{(m)} = \begin{bmatrix} \omega_1^{(m)} & \cdots & 0 & \cdots & 0 \\ \vdots & \ddots & \vdots & \vdots & \vdots \\ 0 & \cdots & \omega_k^{(m)} & \cdots & 0 \\ \vdots & \vdots & \vdots & \ddots & \vdots \\ 0 & \cdots & 0 & \cdots & \omega_N^{(m)} \end{bmatrix} \tag{27}$$

where $\omega_k^{(m)}$ denotes the weight of the k-th sampling point when constructing the m-th BRSM, which can be evaluated by the following equations.

$$\omega_k^{(m)} = \begin{cases} 1 & , m = 1 \\ \dfrac{\omega_k^{(m-1)}}{Z^{(m-1)}} \cdot \left[1 + \exp\left(\lambda \varepsilon_k^{(m-1)}\right)\right], & m = 2, 3, \cdots, M \end{cases} \tag{28}$$

$$\varepsilon_k^{(m-1)} = \frac{\left| RSM^{(m-1)}\left(\boldsymbol{x}^{(k)}\right) - y^{(k)} \right|}{y^{(k)}} \tag{29}$$

$$Z^{(m-1)} = \frac{1}{N} \sum_{k=1}^{N} \omega_k^{(m-1)} \cdot \left[1 + \exp\left(\lambda \varepsilon_k^{(m-1)}\right)\right] \tag{30}$$

where $\omega_k^{(m-1)}$ and $\omega_k^{(m)}$ denote the weight of $\boldsymbol{x}^{(k)}$ when constrcuting the (m-1)-th and the m-th BRSM, respectively; $\varepsilon_k^{(m-1)}$ denotes the relative error of the (m-1)-th BRSM over

$\boldsymbol{x}^{(k)}$; $RSM^{(m-1)}(\boldsymbol{x}^{(k)})$ denotes the predicted response of the (m-1)-th BRSM for $\boldsymbol{x}^{(k)}$; $Z^{(m-1)}$ is the normalization factor of sampling point weights; λ is the scaling factor.

The weight of each BRSM depends on the total error of each BRSM over the entire sampling points. The smaller the total error, the larger the weight of the BRSM. The weight of the m-th BRSM is defined as follows:

$$\varepsilon^{(m)} = \sqrt{\frac{1}{N} \cdot \sum_{k=1}^{N} \left[\mathrm{RSM}^{(m)}\left(\boldsymbol{x}^{(k)}\right) - y^{(k)}\right]^2} \tag{31}$$

$$\alpha^{(m)} = \frac{\exp\left(\tau \cdot \varepsilon^{(m)}\right)}{\sum_{m=1}^{M} \exp\left(\tau \cdot \varepsilon^{(m)}\right)} \tag{32}$$

where $\varepsilon^{(m)}$ is the root mean square error of the m-th BRSM over the entire samples; $RSM^{(m)}(\boldsymbol{x}^{(k)})$ denotes the predicted response of the m-th BRSM for $\boldsymbol{x}^{(k)}$; τ is the scaling factors; $\alpha^{(m)}$ denotes the weight of the m-th BRSM.

The sensitivity information (gradient vector) of $\boldsymbol{x}^{(k)}$ is approximate by the FD, which can be defined as follows:

$$\mathbf{g}_{\boldsymbol{x}_i}^{(k)} = \frac{\widehat{f}\left(\boldsymbol{x}_{i+}^{(k)}\right) - \widehat{f}\left(\boldsymbol{x}_{i-}^{(k)}\right)}{2h} \tag{33}$$

$$\boldsymbol{x}_{i+}^{(k)} = [x_1, \cdots, x_{i-1}, x_i + h, x_{i+1}, \cdots, x_D]^{\mathrm{T}} \tag{34}$$

$$\boldsymbol{x}_{i-}^{(k)} = [x_1, \cdots, x_{i-1}, x_i - h, x_{i+1}, \cdots, x_D]^{\mathrm{T}} \tag{35}$$

where $\mathbf{g}_{\boldsymbol{x}_i}^{(k)}$ denotes the gradient vector of $\boldsymbol{x}^{(k)}$ for the i-th design variable; $\boldsymbol{x}_{i+}^{(k)}$ and $\boldsymbol{x}_{i-}^{(k)}$ are the new sampling points in the compact neighborhood of $\boldsymbol{x}^{(k)}$, which are generated by adding h to the i-th design variable of $\boldsymbol{x}^{(k)}$ and reducing the i-th design variable of $\boldsymbol{x}^{(k)}$ by h, respectively; $\widehat{f}\left(\boldsymbol{x}_{i+}^{(k)}\right)$ and $\widehat{f}\left(\boldsymbol{x}_{i-}^{(k)}\right)$ denote the predicted response of the strong predictor AdaRSM for $\boldsymbol{x}_{i+}^{(k)}$ and $\boldsymbol{x}_{i-}^{(k)}$, respectively.

3.3 NSGA-III for locating Pareto-optimal solutions

NSGA-III algorithm [34, 35] utilizes a reference point-based selection mechanism to select the populations, which can obtain good performance in the case of four or more objectives optimization. By introducing a set of reference points, the population is selected according to the distances between the individuals and the reference points, thereby guiding the population search to approach the reference points. Because the reference points are evenly distributed over the reference hyperplane, the reference point-based selection mechanism can make the population more evenly distributed on the Pareto frontier and the optimization process can better converge to the Pareto-optimal solution set.

The process of locating the Pareto-optimal solution set of multi-objective optimization problem by the NSGA-III is as follows:

Step 1: The initial population containing N individuals is randomly generated, where N is the size of the population.

Step 2: The original population in the current generation is set as the parent population. The parent population goes through random selection, simulated binary intersection, and polynomial mutation operations to generate the offspring population. The size of the offspring population is N.

Step 3: The parent population and the offspring population are combined to form a new population with a population size of $2N$. Then, the fitness function is used to evaluate each individual in the new combined population by calculating the responses (objectives).

Step 4: According to the fitness of each individual, the non-dominated sorting algorithm and reference point-based selection mechanism is used to select N optimal individuals from the new combined population in Step 3 to enter the next generation.

Step 5: Check whether the convergence condition is satisfied (e.g., generations of the population reach the preset maximum threshold). If the convergence condition is satisfied, the selected N optimal individuals in Step 4 is the Pareto-optimal solution set and the optimization process end; otherwise, the selected N optimal individuals in Step 4 is treated as the original population of next generation and redirect to Step 2.

3.4 Data analysis

Sensitivity analysis among process parameters and responses

Sensitivity analysis is applied to identify the important process parameters (design variables) which have significant influences on responses (objectives). It can exclude irrelevant parameters to reduce the dimension of the design space.

Correlation coefficient is implemented to indicate the sensitivity among process parameters and responses, which can be calculated by the following formula.

$$\rho = \frac{\mathrm{Cov}(X, Y)}{\sqrt{\mathrm{Var}(X)\mathrm{Var}(Y)}} = \frac{E[(X - \mu_X)(Y - \mu_Y)]}{\sigma_X \sigma_Y} \tag{36}$$

where $\mathrm{Cov}(X, Y)$ is the covariance of vector X and vector Y; $\mathrm{Var}(X)$ and $\mathrm{Var}(Y)$ are the variance of X and Y respectively; μ_X and μ_Y are the mean of X and Y respectively; σ_X and σ_Y are the standard deviation of X and Y respectively; ρ is the correlation coefficient, which is in the range of [-1, 1]. If $\rho = 0$, it indicates that there is no correlation between the two vectors; if $\rho < 0$, there is a negative correlation between the two vectors; if $\rho > 0$, there is a positive correlation between the two vectors.

Prediction accuracy analysis The response predictor is utilized as the fitness function of NSGA-III algorithm in the multi-objective optimization process. The prediction accuracy of the response predictor influences the optimization results, which may cause the optimization algorithm to not converge. Therefore, the prediction accuracy analysis is verified by evaluating the root mean squared error (RMSE), mean absolute error (MAE), and coefficient of determination (R^2) between the responses calculated by simulation experiments and the responses predicted by the response predictor. These evaluation criteria can be formulated as follows:

$$\mathrm{RMSE}_j = \sqrt{\frac{1}{N_V}\sum_{k=1}^{N_V}\left(\widehat{y}_j^{(k)} - y_j^{(k)}\right)^2} \quad j = 1, 2, \cdots, K \tag{37}$$

$$\mathrm{MAE}_j = \frac{1}{N_V}\sum_{k=1}^{N_V}\left|\widehat{y}_j^{(k)} - y_j^{(k)}\right| \quad j = 1, 2, \cdots, K \tag{38}$$

$$R^2{}_j = 1 - \frac{\sum_{k=1}^{N_V}\left(\widehat{y}_j^{(k)} - y_j^{(k)}\right)^2}{\sum_{k=1}^{N_V}\left(y_j^{(k)} - \overline{y}_j\right)^2} \quad j = 1, 2, \cdots, K \tag{39}$$

where $R\mathrm{MSE}_j$, MAE_j, and $R^2{}_j$ denote the RMSE, MAE, and R^2 of the j-th response (objective), respectively; K denotes the number of the objectives; N_V denotes the number of the sampling points for verification; $\widehat{y}_j^{(k)}$ and $y_j^{(k)}$ denote the j-th response of the k-th sampling point predicted by the corresponding response predictor and calculated by simulation experiment, respectively; $\overline{y}_j$ denotes the mean of the j-th response.

4 Case study

Because of the characteristic of lightweight, customization, good adaptability to variable complex structures, low cost, high efficiency, etc., the plastic injection molding products are widely used in automobile industry such as the bumper, door, and dashboard. The automobile bumper should meet the mechanical and geometric requirement to ensure the necessary protection function as well as the shape consistency and appearance beauty. Therefore, the automobile front bumper is taken as a case study to verify the proposed method.

4.1 Finite element simulation model

An injection plastic product of the automobile front bumper shown in Fig. 4 is taken into consideration. The maximum size of this product is 1800mm × 430mm × 725mm, in which the maximum thickness is 4 mm and the minimum thickness is 2.5 mm.

Considering the complex structure of the product, the multiple gates can achieve better filling. However, the utilization of multiple gates can inevitably cause the generation of weldlines. The valve hot runner system adopts the valve gate controllers to control the opening and closing of each gate, which can realize the sequential filling of the whole cavity. Therefore, it can reduce the stress concentration at the intersection of the melt flow front and effectively eliminate weldlines. The overview of the conventional and valve hot runner system is shown in Fig. 5. The gate locations, the number of gates, and the gate type are determined by the combination of the "gate location" analysis and the "fill" analysis. As shown in Fig. 5, three new gates and corresponding hot runners are added to the valve hot runner system compared to the conventional runner system in order to balance the runners. For the valve hot runner system, the flow path of the melted plastic in each runner is as follows: hot sprue → hot runner → hot runner → hot gate → cold runner → cold runner → cold gate.

The details of numerical simulation are shown in Table 2. The numerical simulations are executed through the Autodesk® Moldflow® software (version 2018) [36], where the processor of the computer is Inter® Core™ i9-9900K CPU @ 3.60 GHz. The material, acrylonitrile butadiene styrene (ABS), is used to manufacture the product, and its properties are listed in Table 3.

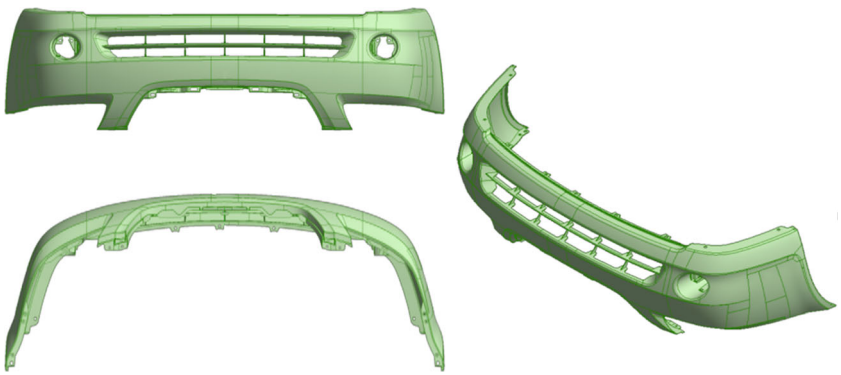

Fig. 4 The 3D model of the automobile front bumper

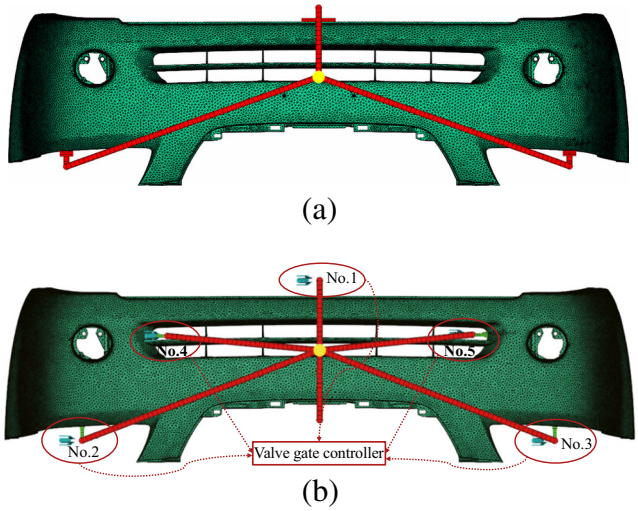

Fig. 5 Overview of the hot runner system. **a** Conventional hot runner system; **b** valve hot runner system

Table 3 Material property of acrylonitrile butadiene styrene (ABS)

Property	Value
Melt/Solid density [**g**/**cm**^{3}]	0.91407/1.0177
Eject temperature [°**C**]	220
Maximum shear stress [MPa]	0.3
Elastic module [GPa]	2.24
Shear module [MPa]	804.6
Poisson ratio	0.392
Thermal conductivity (66 °**C**) [**W**/(**m**· °**C**)]	0.13
Specific heat (85 °**C**) [**J**/(**kg**· °**C**)]	1756
Material characteristics	Amorphous
Recommended mold temperature [°**C**]	40–80
Recommended melt temperature [°**C**]	230–250

4.2 Numerical result analysis

4.2.1 Sensitivity analysis for process parameters

The correlation coefficient can show sensitivity among the design variables and responses, which has been calculated and displayed in Fig. 6. As shown in Fig. 6, the value in each sub-box is the correlation coefficient of the two crossed variables. The positive value indicates the positive correlation, while the negative value indicates the negative correlation, and zero value indicates irrelevance. The bigger the absolute value of the correlation coefficient is, the stronger the relationship between the two variables is.

According to the heat-map plot in Fig. 6, it can be found that t_{inj}, P_{p1}, and t_c have the negative influence on warpage with the correlation coefficients equaling to −0.86, −0.5, and −0.28, respectively; T_{melt} has the positive influence on warpage with the correlation coefficient equaling to 0.18. Similarly, T_{melt} and t_{p1} have the positive influence on minimum weldline temperature with the correlation coefficients equaling to 0.96 and 0.27, respectively; t_{inj}, P_{p1}, and t_{p2} have the negative influence on minimum weldline temperature with the correlation coefficients equaling to −0.12, −0.19, and −0.27, respectively. P_{p1}, T_{melt}, t_{p1}, and t_{p2} have the positive influence on clamping force with the correlation coefficients equaling to 0.92, 0.2, 0.15, and 0.1, respectively; t_{inj} and t_c have the negative influence on clamping force with the correlation coefficients equaling to −0.17 and −0.22, respectively. In fact, cycle time is the sum of t_{inj}, t_{p1}, t_{p2}, and t_c. It indicates that t_{inj}, t_{p1}, t_{p2}, and t_c have a significant positive influence on cycle time. In addition, the correlation coefficients between warpage and cycle time are −0.48, which indicates that cycle time changes in the opposite direction with warpage.

Table 2 Detailed settings of the numerical simulations in Moldflow

	Mesh type	Dual domain
Mesh	Element	Type: triangle Count: 104866
	Aspect ratio	Maximum: 14.96 Minimum: 1.16 Average: 1.61
	Match percentage	Match percentage: 91.8% Reciprocal percentage: 88.4%
Boundary conditions	Valve gate controller	Valve gate trigger: flow front Trigger location: specific node
	Cooling	Coolant: pure water Coolant inlet temperature: 25 °C
Injection molding machine	Maximum machine injection pressure	180 MPa
	Maximum machine clamp force	7000.22 tonne

4.2.2 Accuracy analysis for response prediction

Fifteen experiments different from thirty-six initial sampling points, which are both generated by the Latin hypercube sampling (LHS), are implemented to verify the prediction accuracy of the response predictors. The cycle time is the sum of the injection time, packing time ,and cooling time, which can be accurately calculated based on the design variables of the four-objective optimization problem. The proposed GERSM, classical RSM, Kriging, support vector regression (SVR), and Gaussian process regression (GPR) are applied to construct

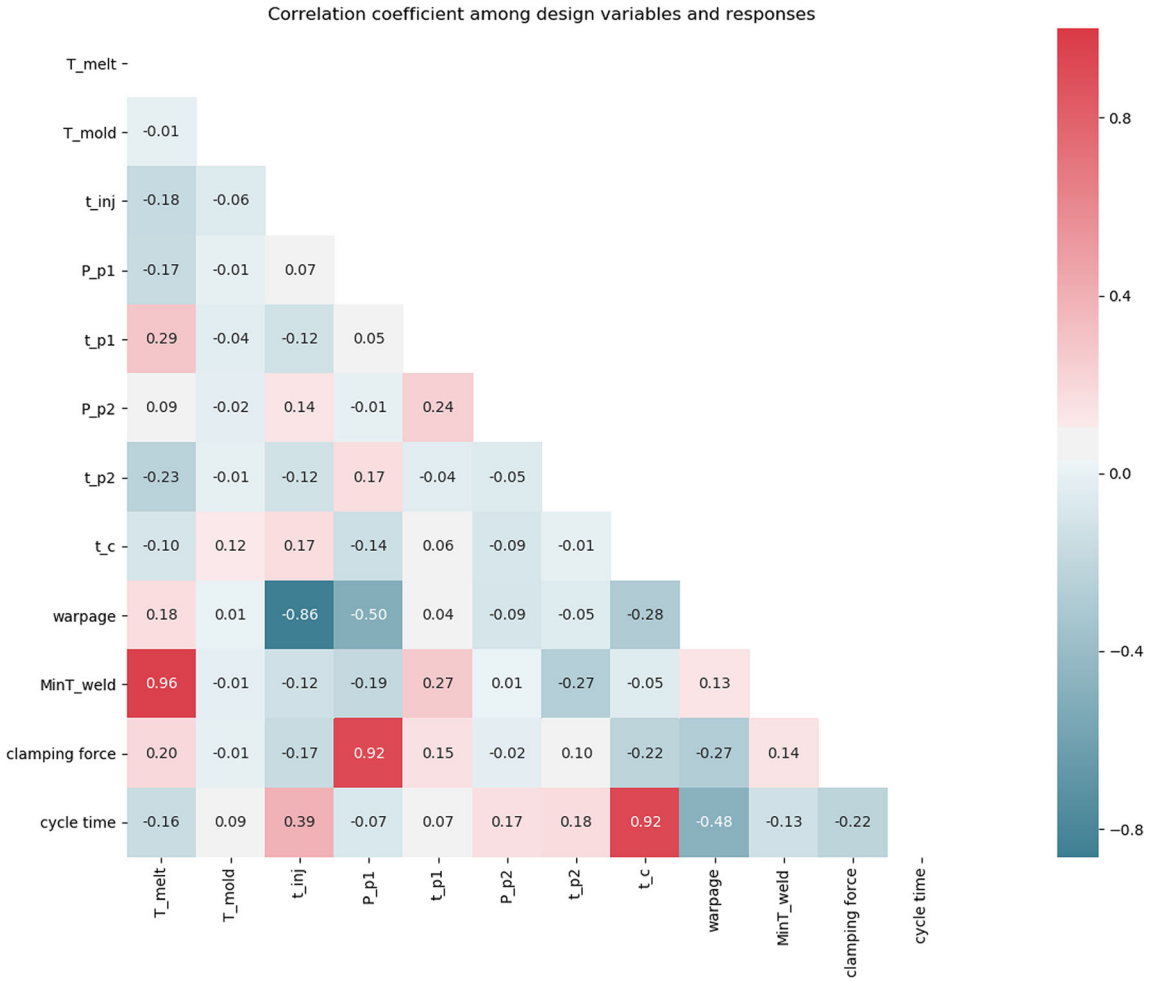

Fig. 6 Correlation relationship among the design variables and responses

the surfaces of design variables and responses (warpage, minimum weldline temperature, and clamping force). The prediction results of responses are displayed in Fig. 7, from which it can be found that Kriging has the largest prediction error, while the proposed model works best.

As shown in Fig. 7, the predictions and experiments of the responses are qualitatively compared. In order to quantitatively compare the performance of different prediction models, MSE, RMSE, MAE, and R^2 are applied to evaluate the performance of the prediction models, which are calculated and displayed in Tables 4, 5, and 6.

The smaller the MAE and RMSE are, the higher the prediction accuracy of model is. $R^2 \in [0, 1]$ is closer to 1; the accuracy of model is higher. As shown in Tables 4, 5, and 6, it can be found that the proposed model has the highest prediction accuracy for the warpage, minimum weldline temperature, and clamping force, compared with RSM, SVR, GPR, and Kriging.

4.2.3 Multi-objective optimization results

NSGA-III algorithm is implemented to locate the Pareto-optimal solutions for the four-objective optimization problem. The parameters of this algorithm are set as follows:

Population size = 220	Generation = 600	Refrence point division = 9
Crossover possibility = 1.0	Distribution index of crossover = 30	
Mutation possibility = 0.2	Distribution index of mutation = 20	

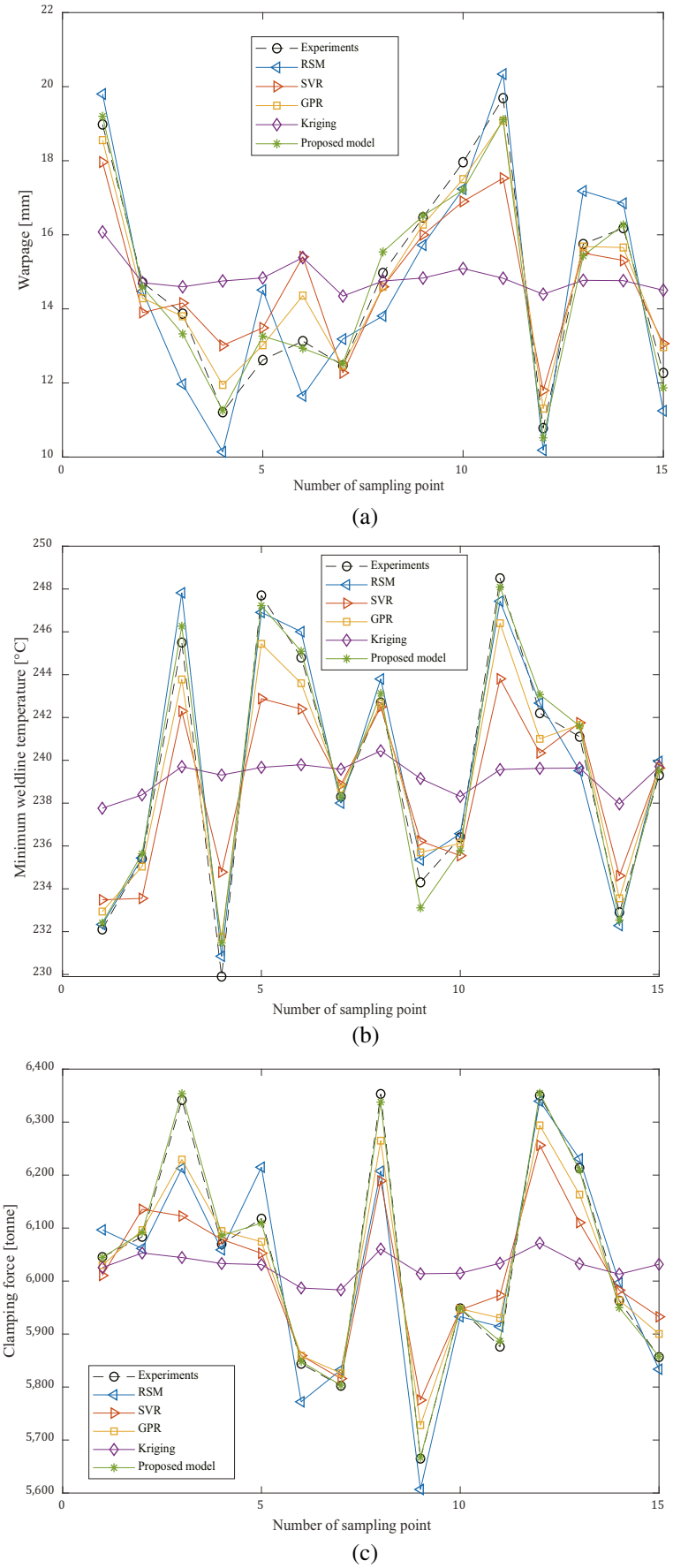

Fig. 7 Comparison of prediction models and experiments. **a** Warpage; **b** minimum weldline temperature; **c** clamping force

Table 4 Comparison of different prediction models (warpage)

Model	Evaluation criteria		
	MAE	RMSE	R^2
RSM	1.0081	1.1114	0.8256
SVR	0.9495	1.1436	0.8153
GPR	0.4492	0.5405	0.9588
Kriging	2.0905	2.4586	0.1465
Proposed model	0.3216	0.3977	0.9777

Table 6 Comparison of different prediction models (clamping force)

Model	Evaluation criteria		
	MAE	RMSE	R^2
RSM	50.245	65.1029	0.8998
SVR	71.724	93.3427	0.7939
GPR	40.3412	50.717	0.9392
Kriging	156.2955	188.239	0.1619
Proposed model	6.7691	8.6446	0.9982

The triple-objective Pareto frontiers among warpage, minimum weldline temperature, clamping force, and cycle time are shown in Fig. 8, and the pair-wise Pareto frontiers are shown in Fig. 9. As shown in Fig. 8, the triple-objective Pareto frontiers show that any three of four objectives cannot reach the optimal at the same time. Therefore, different process parameters have different influences on the results. The four objectives cannot reach the optimal result at the same time and the ideal solution of the optimization problem cannot be located, which leads to the trade-off.

The pair-wise Pareto frontier shown in Fig. 9a indicates that there is no obvious trade-off between warpage and $MinT_{\mathrm{weld}}$ (minimum weldline temperature). Observing Fig. 6, warpage is strongly influenced by t_{inj} and P_{p1}, while $MinT_{\mathrm{weld}}$ is strongly influenced by T_{melt}.

The pair-wise Pareto frontier shown in Fig. 9b indicates a trade-off between warpage and clamping force. Observing Fig. 6, the correlation coefficient between warpage and clamping force equals to −0.27, which means that they are negatively correlated and change in reverse direction. As shown in Fig. 6, P_{p1} has reverse impact on warpage and clamping force, with correlation coefficients equaling to −0.5 and 0.92, respectively. It means that smaller P_{p1} leads to smaller clamping force, but larger warpage. They cannot reach the optimal at the same time.

The pair-wise Pareto frontier shown in Fig. 9c indicates an obvious trade-off between warpage and cycle time. Observing Fig. 6, the correlation coefficient between warpage and cycle time equals to −0.48, which means that they are negatively correlated and change in reverse direction. As shown in Fig. 6, t_c and t_{inj} have reverse impact on warpage and cycle time. It means that shorter t_c and t_{inj} lead to shorter cycle time, but larger warpage. They cannot reach the optimal at the same time.

The pair-wise Pareto frontier shown in Fig. 9d indicates a trade-off between $MinT_{\mathrm{weld}}$ and clamping force. Observing Fig. 6, the correlation coefficient between $MinT_{\mathrm{weld}}$ and clamping force equals to 0.14, which means that they are positively correlated and change in same direction. Therefore, clamping force and the opposite of minimum weldline temperature ($-MinT_{\mathrm{weld}}$) change in reverse direction. As shown in Fig. 6, T_{melt}, t_{inj}, and t_{p1} have same impact on $MinT_{\mathrm{weld}}$ and clamping force. It means that smaller T_{melt}, larger t_{inj}, and smaller t_{p1} lead to smaller clamping force and $MinT_{\mathrm{weld}}$. However, the melted plastic will be quickly solidified with the low weldline temperature, which causes the generation of long weldlines. Therefore, smaller $MinT_{\mathrm{weld}}$ generates larger weldlines. They cannot reach the optimal at the same time to simultaneously minimize the weldlines and clamping force.

The pair-wise Pareto frontier shown in Fig. 9e indicates that there is no obvious trade-off between $MinT_{\mathrm{weld}}$ and cycle time. Observing Fig. 6, $MinT_{\mathrm{weld}}$ is strongly influenced by T_{melt}, while cycle time is strongly influenced by t_{inj}, t_{p1}, t_{p2}, and t_c.

The pair-wise Pareto frontier shown in Fig. 9f indicates that there is no obvious trade-off between clamping force and cycle time. Observing Fig. 6, clamping force is strongly influenced by P_{p1}, while cycle time is strongly influenced by t_{inj}, t_{p1}, t_{p2}, and t_c.

The Pareto-optimal solutions located by NSGA-III are listed in Table 7. The trade-off analysis is performed

Table 5 Comparison of different prediction models (minimum weldline temperature)

Model	Evaluation criteria		
	MAE	RMSE	R^2
RSM	0.8372	1.0178	0.9675
SVR	2.0885	2.6094	0.7862
GPR	1.0145	1.2283	0.9526
Kriging	4.3754	5.1702	0.1606
Proposed model	0.5505	0.6769	0.9856

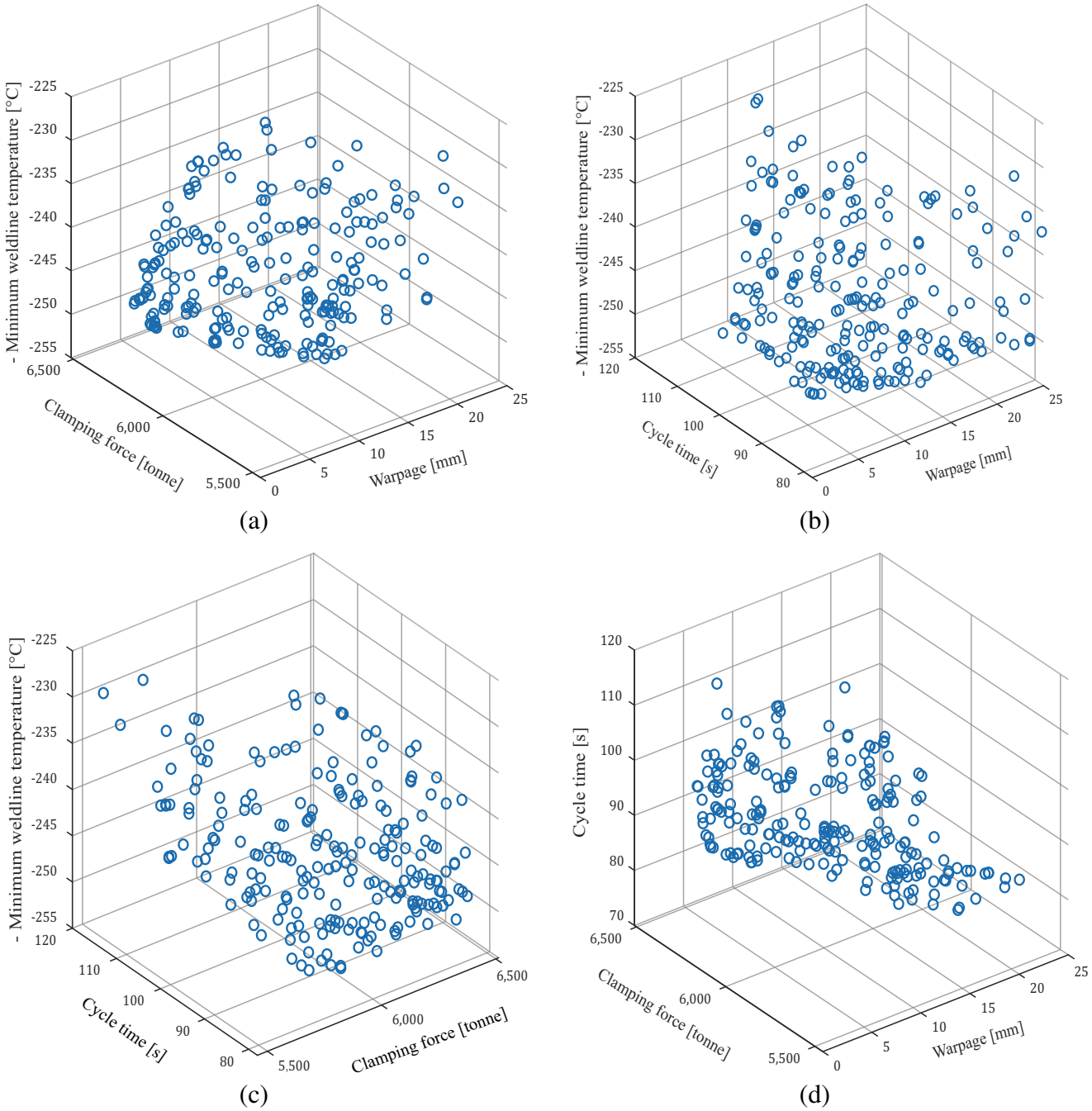

Fig. 8 Triple-objective Pareto frontiers. **a** Warpage and minimum weldline temperature and clamping force; **b** warpage and minimum weldline temperature and cycle time; **c** minimum weldline temperature and clamping force and cycle time; **d** warpage and clamping force and cycle time

to determine the better and worse solution for decision-making based on the spider-web chart. The ideal and nadir value of the objectives in Eq. (3) can be set as follows: $\left[f_1^I, f_2^I, f_3^I, f_4^I\right] = [0, -255, 5400, 75]$; $\left[f_1^N, f_2^N, f_3^N, f_4^N\right] = [25, -225, 7000, 115]$. In the spider-web chart, the areas of the Pareto-optimal solutions located by NSGA-III are calculated and displayed in Table 8, where there is no preference for all objective.

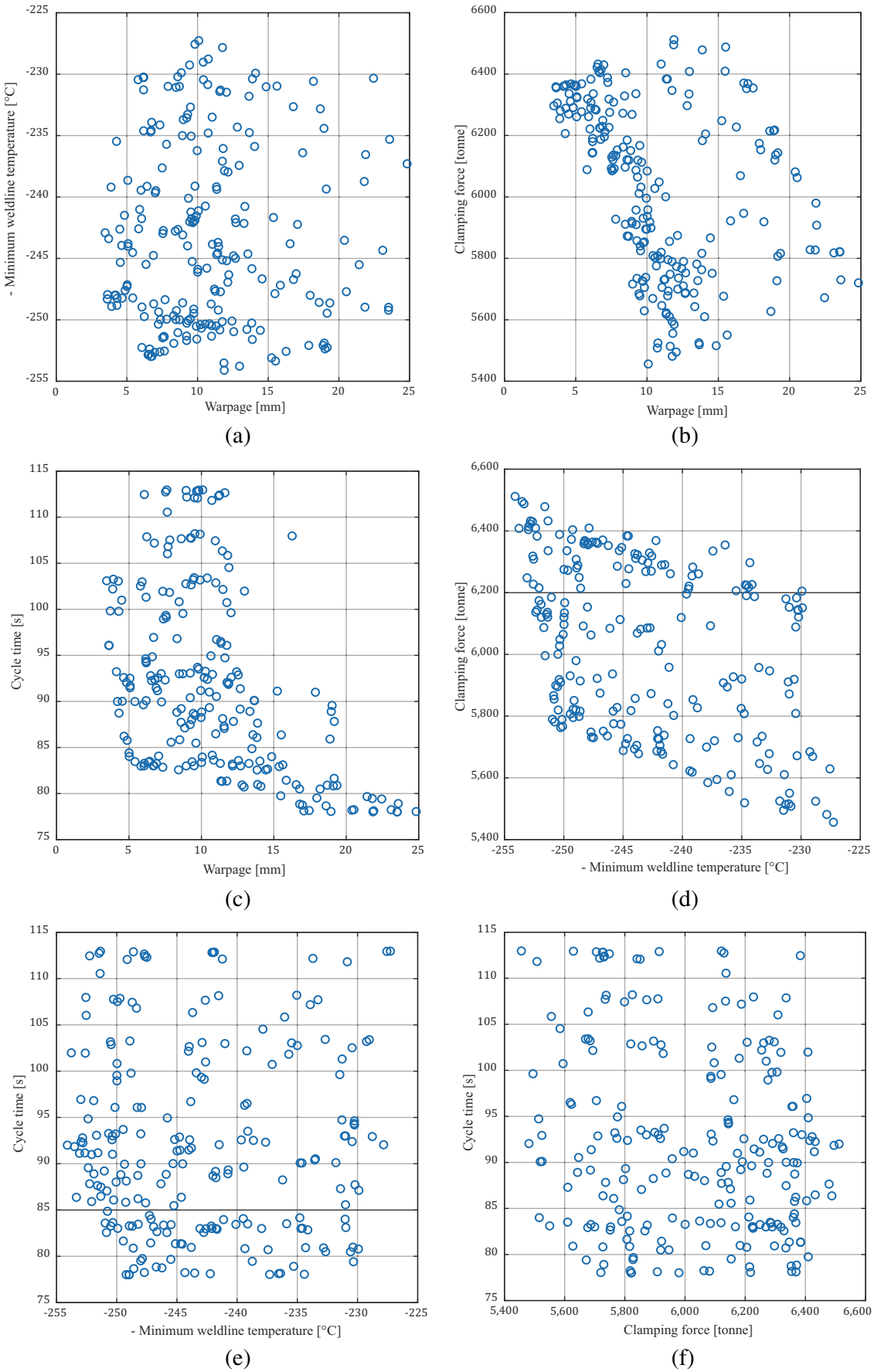
- Minimum weldline temperature [°C]
Warpage [mm]
(a)
Clamping force [tonne]
Warpage [mm]
(b)
Cycle time [s]
Warpage [mm]
(c)
Clamping force [tonne]
- Minimum weldline temperature [°C]
(d)
Cycle time [s]
- Minimum weldline temperature [°C]
(e)
Cycle time [s]
Clamping force [tonne]
(f)

◀ **Fig. 9** Pair-wise Pareto frontiers. **a** Warpage and minimum weldline temperature; **b** warpage and clamping force; **c** warpage and cycle time; **d** minimum weldline temperature and clamping force; **e** minimum weldline temperature and cycle time; **f** clamping force and cycle time

The smaller the area of alternative solution, the better the solution.

The spider-web chart is shown in Fig. 10, in which the red, blue, and black lines represent the better solution, worse solution, and alternative solutions, respectively. As shown in Fig. 10, the area of the better solution is smaller than that of the worse solution. In addition, warpage and weldlines temperature distribution at the better and worse solution are compared and displayed in Figs. 11 and 12, respectively. As shown in Fig. 11, it can be found that warpage is well reduced at better solution compared to that at worse solution. As shown in Fig. 12, it can be found that weldlines are well reduce at better solution compared to that at worse solution. From the perspective of process parameters, it can indicate that larger packing pressure and injection time can reduce warpage.

To verify the effect of the valve hot runner system on the weldline reduction, the comparison of weldlines under the conventional hot runner system and under the valve hot runner system at better solution is shown in Fig. 13. It can be found that the weldlines are generated in inconspicuous positions such as grilles, lamp holes, and product edges and effectively eliminated when valve hot runner system is used, compared with conventional hot runner system. The surface quality of the automobile front bumper is higher when the valve hot runner system is applied.

According to the result of the trade-off analysis, the optimized setting of the process parameters is shown in Table 9 for the product quality and productivity improvement and the cost-saving. The warpage and the weldlines of the automobile front bumper after the optimization are compared with them before the optimization, as shown in Fig. 14. Moreover, the setting of the process parameters is determined by the recommendation of Moldflow and the result of the "molding window" analysis.

The verification of prediction accuracy for four objectives at optimized solution is summarized in Table 10, which shows that relative absolute errors for all objectives

Table 7 Pareto-optimal solutions located by NSGA-III

No.	Process parameters							
	T_{melt}[°C]	T_{mold}[°C]	t_{inj}[s]	P_{p1}[MPa]	P_{p2}[MPa]	t_{p1}[s]	t_{p2}[s]	t_c[s]
1	245.37	40.99	8	102.22	69.86	20	35.05	20.14
2	250	44.87	7.26	108.29	40.04	20.24	39.97	20
3	249.66	78.99	5.91	100	70	20.08	35	20.66
196	249.98	40.02	8	108.85	70	20.28	35	20
203	230	79.74	4.40	100.68	40.13	20	35	20
220	238.19	40	3.05	110	69.90	20.10	35	20

Table 8 Areas of Pareto-optimal solutions in spider-web chart

No.	Objective responses				Area	Decision making
	Warpage [mm]	Minimum weldline temperature[°C]	Clamping force [tonne]	Cycle time [s]		
1	12.1400	246.94	5874.5	93.19	0.1852	
2	9.2190	251.32	6336.0	87.48	0.2073	
3	19.1652	249.45	5806.7	81.65	0.1792	
196	6.2652	248.96	6307.8	83.28	0.1655	Better
203	22.4501	230.33	5671.8	79.41	0.4978	Worse
220	17.4395	236.40	6354.5	78.16	0.4523	

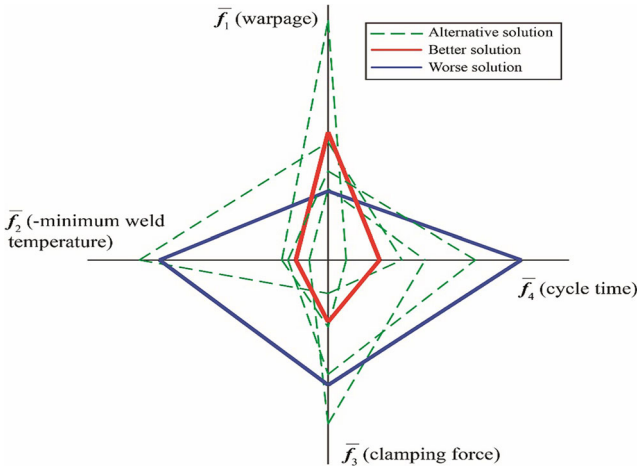

Fig. 10 Spider-web chart at better and worse solution

at optimized solution are below 2.5%. With the result of accuracy analysis displayed in Section 4.2.1, the prediction accuracy can be confirmed and verified.

The proposed multi-objective optimization method analyzes the correlation between the process parameters and the objectives and conducts the trade-off analysis to balance the multiple conflicting objectives. It can effectively locate the optimized process parameters setting to achieve the product quality and productivity improvement and the cost-saving, which can provide a theoretical basis and reference for the actual injection molding process.

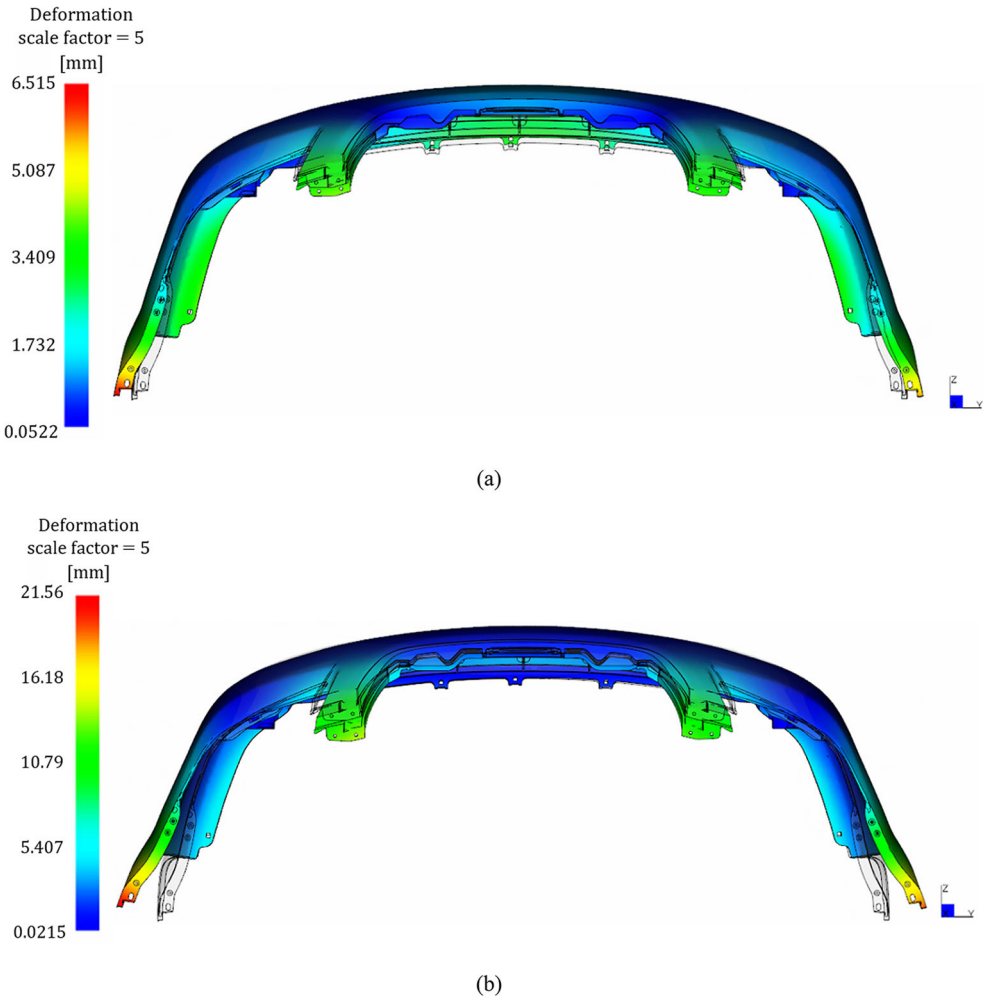

Fig. 11 Comparison of warpage at better and worse solution. **a** Better solution; **b** worse solution

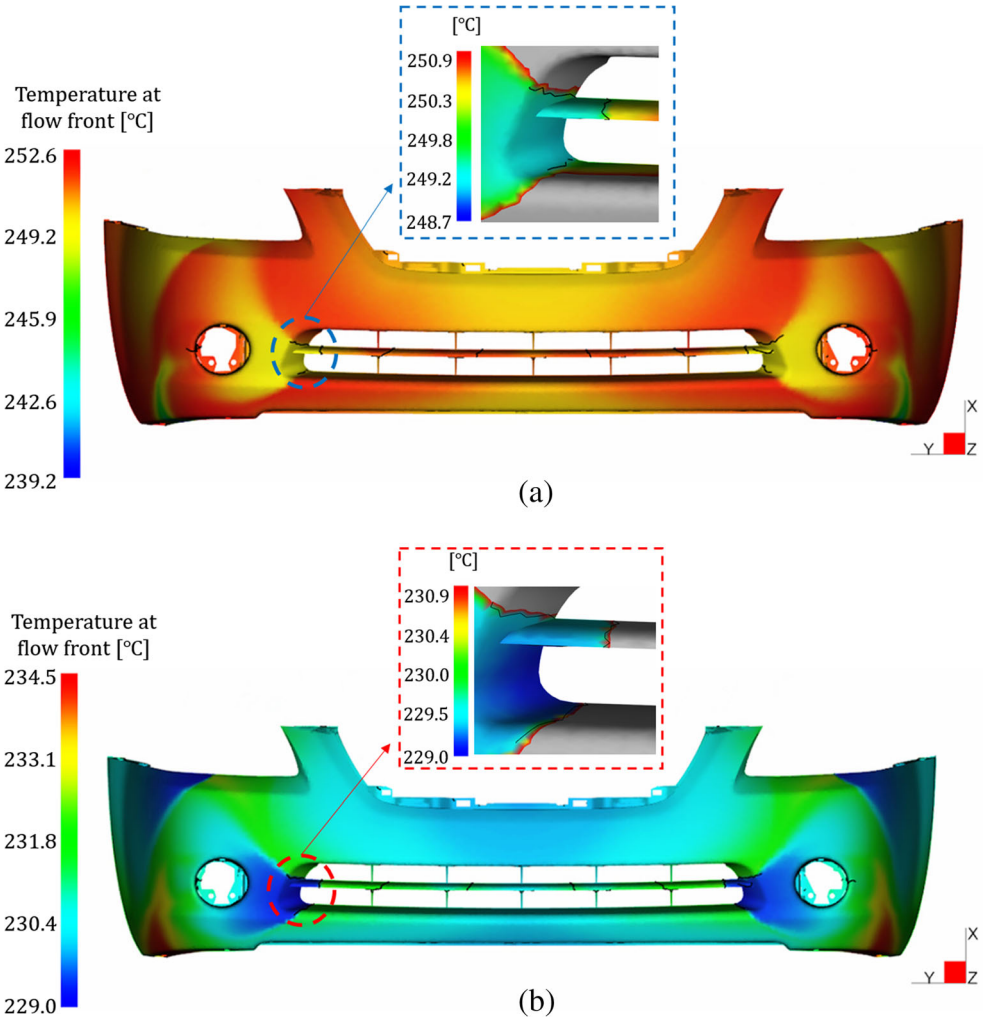

Fig. 12 Comparison of weldline temperature distribution at better and worse solution. **a** Better solution; **b** worse solution

5 Conclusion

In this paper, the multi-objective optimization of process parameters in PIM for minimizing the warpage, weldlines, clamping force, and cycle time is performed to realize high product quality, high productivity, and low energy consumption. The melted plastic will be quickly solidified with low weldline temperature and long weldlines will generate. To shorten the weldlines, the minimum weldline temperature is considered to be maximized. In this view, we propose a differential sensitivity fusion method (DSFM). The conclusions are as follows:

(1) The variable packing pressure profile and the melt temperature, mold temperature, injection time, and cooling time are taken as design variables and optimized. The generic optimization algorithm NSGA-III is applied to locate the Pareto-optimal solutions. Pareto frontier shows that selected four objectives cannot simultaneously reach the optimal, which leads

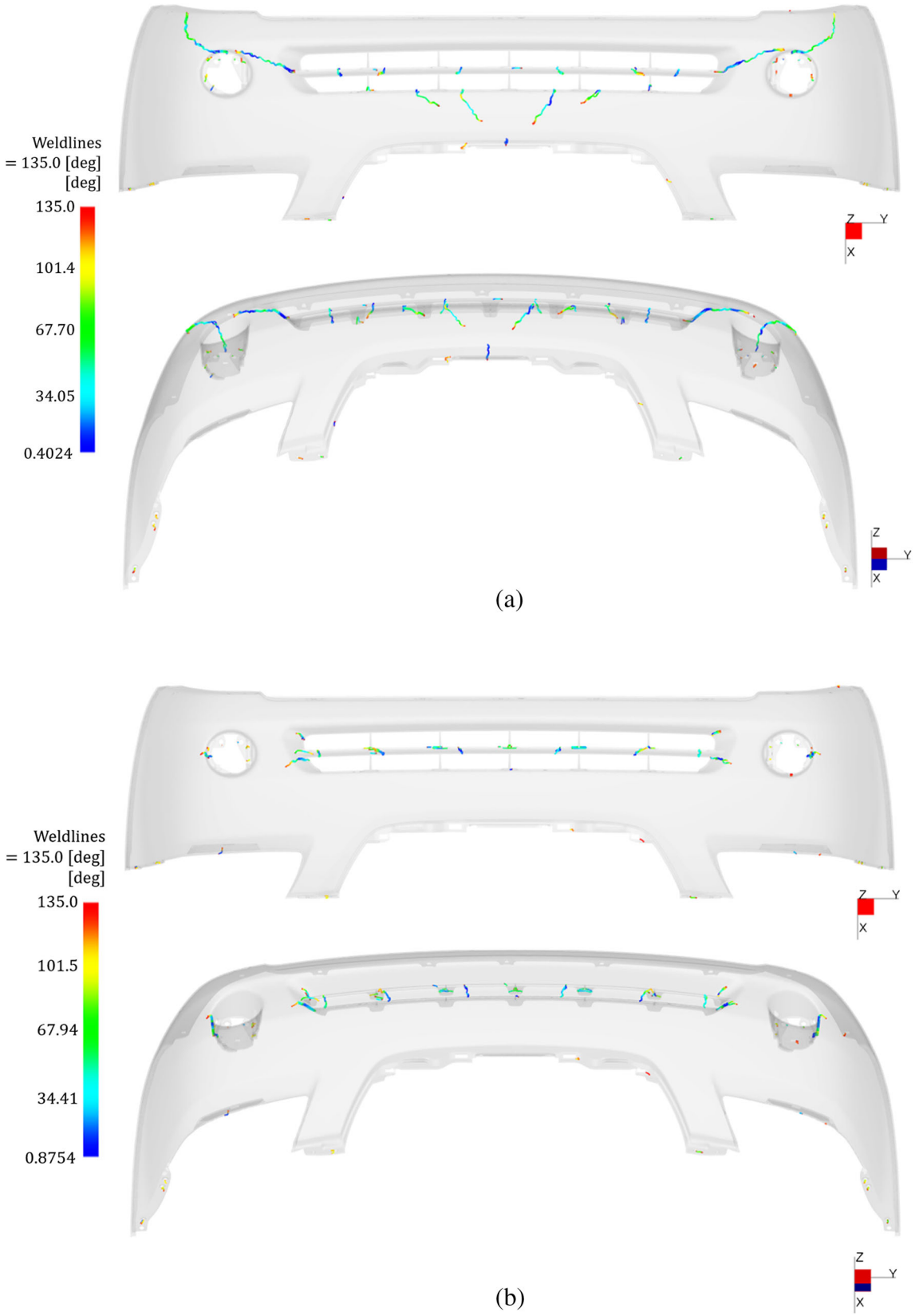

Fig. 13 Comparison of weldlines at better solution. **a** Conventional hot runner system; **b** valve hot runner system

Table 9 The optimized setting of the process parameters based on the trade-off analysis

Solution	Setting of process parameters		Responses of objectives	
	Parameter	Value	Objective	Value (simulation)
Before optimization	T_{melt}[°C]	245.56	Warpage [mm]	14.53
	T_{mold}[°C]	80		
	t_{inj}[s]	5.69	Minimum weldline temperature[°C]	244.9
	P_{p1}[MPa]	105		
	P_{p2}[MPa]	55	Clamping force [tonne]	6096.3
	t_{p1}[s]	22.5		
	t_{p2}[s]	37.5	Cycle time [s]	95.69
	t_c[s]	30		
After optimization	T_{melt}[°C]	249.83	Warpage [mm]	12.89
	T_{mold}[°C]	40.02		
	t_{inj}[s]	8	Minimum weldline temperature[°C]	249.7
	P_{p1}[MPa]	101.15		
	P_{p2}[MPa]	68.68	Clamping force [tonne]	5850.0
	t_{p1}[s]	20.68		
	t_{p2}[s]	35	Cycle time [s]	87.06
	t_c[s]	23.38		

to the trade-off. The spider-web chart is used to perform the trade-off analysis among the four objectives, and the better and worse solutions are identified for decision-making.

(2) The metamodeling method, GERSM coupling with the MLSM, is used to construct the response predictors, which fit the mathematical relationship between design variables and responses and is taken as the fitness functions in the multi-objective optimization process. This model simultaneously utilizes the response and sensitivity information of the sampling point to improve the accuracy of the response predictors. Considering the capture of the sensitivity information, ASGM is proposed to calculate the gradient vector for each design variable of the sampling point. The results of the accuracy analysis for response predictors show that the proposed model has the highest prediction accuracy for the warpage, minimum weldline temperature, and clamping force, compared with RSM, SVR, GPR, and Kriging.

(3) The automobile bumper is taken as the case study, where the valve hot runner system is used. The numerical simulation result shows that the weldlines are generated in inconspicuous positions such as grilles, lamp holes, and product edges and effectively eliminated, compared with the conventional hot runner system. The valve hot runner system can effectively improve the product quality.

Author contribution Huifang Zhou's contributions are conceptualization; writing—original draft; methodology; formal analysis; investigation; and project administration. Shuyou Zhang's contributions are Investigation; resources; and validation. Zili Wang's contributions are funding acquisition; project administration; methodology; formal analysis; supervision; visualization; and writing—review and editing.

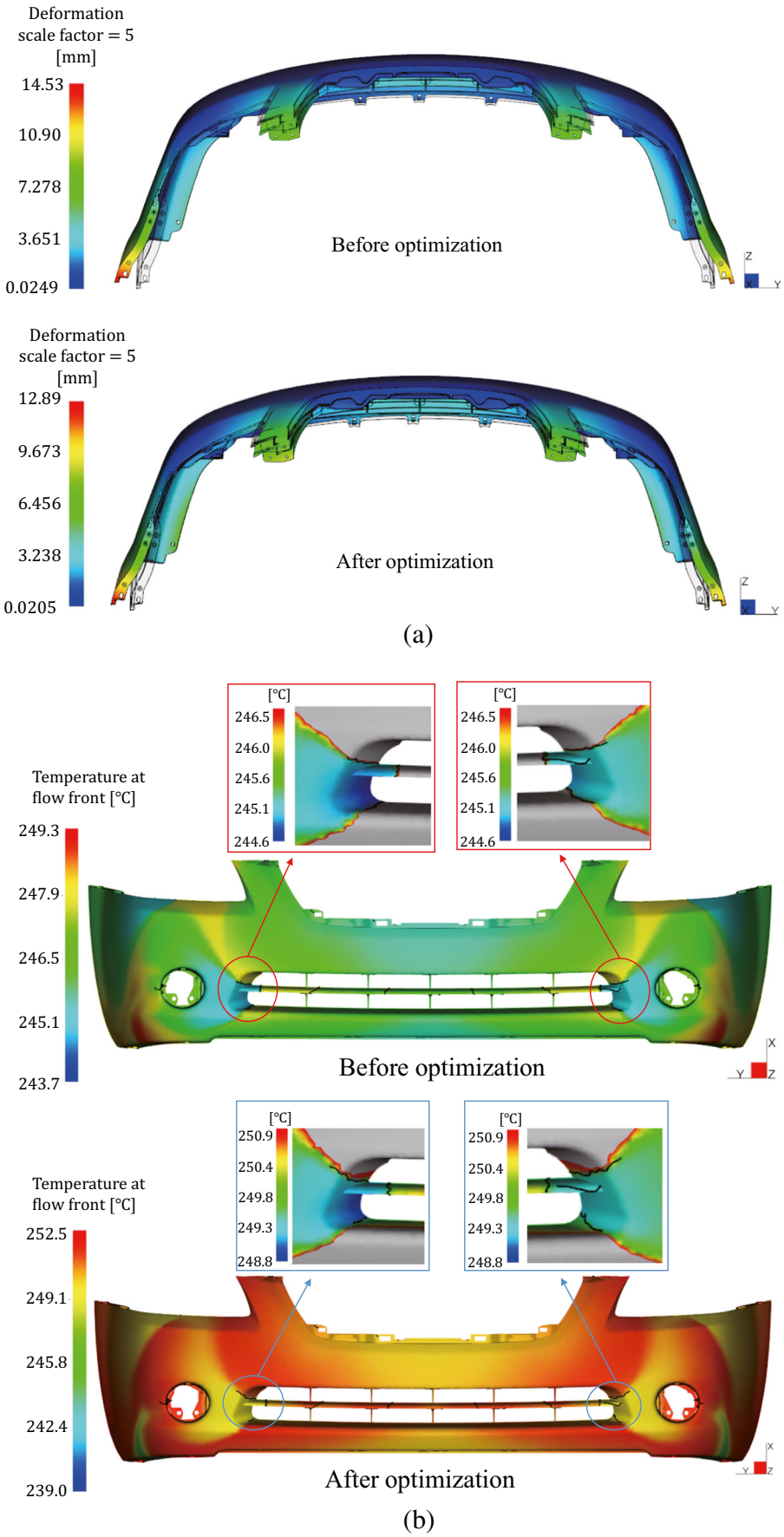

Fig. 14 The warpage and weldlines of the automobile front bumper before and after optimization. **a** Warpage; **b** weldlines

Table 10 Verification of the optimized results

Solution		Objectives			
		Warpage [mm]	Minimum weldline temperature [°C]	Clamping force [tonne]	Cycle time [s]
Optimized results	Prediction	12.58	250.82	5855.2	87.06
	Simulation	12.89	249.7	5850.0	87.06
Error (RAE)		2.40%	0.45%	0.089%	0%

Funding This work has been funded by the National Natural Science Foundation of China (51905476).

Declarations

Ethics approval and consent to participate No applicable

Consent for publication Authors consent to publish this article.

Competing interests The authors declare no competing interests.

Appendix

The sampling points for constructing and training the response predictor are displayed in Table 11, and the objective responses of them are displayed in Table 12. The sampling points for confirmation or validation are displayed in Table 13, and the objective responses of them are displayed in Table 14.

Table 11 Sampling points for training generated by LHS

No.	Design variables							
	T_{melt}[°C]	T_{mold}[°C]	t_{inj}[s]	P_{p1}[MPa]	P_{p2}[MPa]	t_{p1}[s]	t_{p2}[s]	t_c[s]
1	245.0414	55.0286	6.0794	107.5965	53.4387	23.9714	36.4930	32.4443
2	234.0339	70.1833	3.4851	109.0192	56.6081	20.8847	39.4706	27.7306
3	231.9070	43.9229	7.5325	109.5236	55.0104	24.5062	37.7661	26.7098
4	245.5729	77.3180	4.0796	107.3598	46.7311	20.6767	39.0929	21.6369
5	242.3197	42.7747	5.7035	100.1422	44.5298	21.6432	35.5832	21.9294
6	230.0224	59.8606	5.3209	100.4173	43.8071	22.4999	39.3418	32.1562
7	249.0854	40.9641	3.6849	101.1289	66.3851	22.3030	35.2581	23.6777
8	240.9002	72.3661	3.1271	101.8363	48.5661	23.1266	39.6614	30.6595
9	241.4019	68.2189	7.1572	100.8008	64.1553	22.7556	39.8124	37.0866
10	241.7156	46.3719	6.9709	103.8221	62.1883	21.7129	37.9891	33.9531
11	244.9917	66.8169	4.6495	103.1431	64.2311	20.8308	35.7517	32.9374
12	247.6907	64.3799	3.2162	105.8780	67.8779	23.4556	36.0909	38.1233
13	238.6269	75.0469	5.5140	109.1750	46.2718	20.9789	38.4854	35.4173
14	231.3650	64.7531	3.7842	102.4402	51.2529	22.7811	39.2166	31.5262
15	244.4113	78.5122	6.5944	102.5666	69.7425	24.4402	35.3940	37.3515
16	236.8566	56.2209	5.1432	108.1711	60.8743	20.4870	38.8103	21.0834
17	246.7280	51.6367	4.1285	102.9436	66.6817	24.7413	39.8706	22.9526
18	237.7169	61.2286	7.9516	101.5250	54.5720	20.1052	37.1135	39.0998
19	246.4235	50.2463	6.8831	105.6957	41.6728	24.0508	38.2381	34.5852
20	233.7332	79.9229	7.7025	107.8746	60.4535	24.1926	37.2964	28.9015
21	232.2304	60.8014	3.4060	103.4045	47.9783	20.3293	36.3527	33.6756
22	247.9951	49.5785	3.8694	106.8606	57.3223	22.0830	38.9487	26.5221

Table 11 (continued)

No.	Design variables							
	T_{melt}[°C]	T_{mold}[°C]	t_{inj}[s]	P_{p1}[MPa]	P_{p2}[MPa]	t_{p1}[s]	t_{p2}[s]	t_c[s]
23	230.9701	56.8170	6.6866	106.6418	63.1723	24.6695	38.7154	24.5125
24	243.2597	69.5334	6.2405	104.4928	58.4727	21.4022	36.7612	22.3299
25	243.5861	54.1779	7.2084	105.4473	57.7278	23.7944	38.0679	25.2994
26	239.5401	44.8915	4.8651	109.7846	52.8919	22.5863	37.5159	20.5050
27	237.8683	76.1340	4.7182	101.0613	49.3091	23.5233	35.4452	28.5754
28	249.5370	65.6683	5.7948	102.1918	52.0734	23.7162	35.0103	24.3403
29	239.3313	52.2948	7.3525	104.1930	41.2067	20.1984	37.8918	38.5935
30	240.2531	47.9801	5.9340	106.1455	59.8223	21.1136	36.5948	30.3583
31	232.8473	46.9901	5.0184	108.6112	68.6768	22.9375	36.9962	36.4918
32	236.5994	62.5075	4.3693	105.0377	45.7144	21.9051	36.8176	25.7074
33	235.6354	57.8892	6.4628	104.1564	43.2898	24.9052	35.8800	28.0468
34	248.3890	72.1497	4.4286	107.0709	65.2639	23.2836	37.4459	35.6719
35	234.8790	41.8490	5.4572	104.7229	50.3262	22.0851	38.3694	39.8864
36	235.5128	74.4396	7.7679	108.4692	40.6503	21.3772	36.1364	29.6233

Table 12 Numerical simulation results of responses for sampling points in Table 11

No.	Warpage [mm]	Minimum weldline temperature [°C]	Clamping force [tonne]	Cycle time [s]
1	12.09	244.4	6247.7	98.9880
2	16.35	233.5	6278.8	91.5710
3	9.18	231.1	6163.2	96.5145
4	16.00	245.1	6270.3	85.4861
5	18.69	241.7	5765.4	84.8593
6	17.37	229.2	5631.6	99.3188
7	20.66	248.6	5906.0	84.9238
8	20.11	240.2	5888.7	96.5746
9	12.55	240.7	5740.8	106.8118
10	12.11	241.2	5949.8	100.6260
11	17.29	244.4	5989.2	94.1695
12	16.93	247.1	6191.1	100.8860
13	12.10	238.0	6295.2	100.3955
14	19.49	230.8	5822.2	97.3082
15	13.06	244.0	5906.9	103.7801
16	14.87	236.2	6230.6	85.5238
17	18.99	246.1	5997.0	91.6930
18	10.78	237.4	5707.5	104.2700
19	10.92	245.9	6119.5	103.7571
20	9.343	233.0	6076.3	98.0929
21	19.19	231.5	5902.9	93.7637
22	16.28	247.6	6254.6	91.4232
23	12.44	230.3	6001.7	94.5840
24	14.80	242.6	6039.3	86.7338
25	11.35	242.9	6073.7	94.3702
26	14.61	238.9	6364.6	85.4723
27	19.26	237.1	5791.8	92.2622

Table 12 (continued)

No.	Warpage [mm]	Minimum weldline temperature [°C]	Clamping force [tonne]	Cycle time [s]
28	16.68	248.8	5953.9	88.8616
29	10.76	238.7	5928.6	104.0362
30	13.54	239.7	6114.6	94.0007
31	13.86	232.1	6203.7	101.4440
32	17.81	236.1	6040.1	88.7993
33	13.90	235.0	5916.9	95.2948
34	14.83	247.7	6261.7	100.8300
35	14.24	234.2	5965.1	105.7982
36	9.098	234.8	6143.5	94.9048

Table 13 Sampling points for validation generated by LHS

No.	Design variables							
	T_{melt}[°C]	T_{mold}[°C]	t_{inj}[s]	P_{p1}[MPa]	P_{p2}[MPa]	t_{p1}[s]	t_{p2}[s]	t_c[s]
1	232.6232	61.0117	3.3646	105.5334	42.4424	22.7746	37.0280	27.1901
2	235.9184	62.4280	5.3734	106.2410	59.1531	22.5703	38.3329	30.4110
3	246.1575	58.0635	4.7274	108.6443	41.8184	24.4427	35.1792	36.3488
4	230.4411	54.9743	6.9131	107.9541	45.4671	20.4350	39.8586	26.3429
5	248.4128	78.4454	6.1352	105.1203	53.6927	20.9773	36.1797	37.4434
6	245.5081	41.9952	7.6592	101.6461	47.4380	21.2484	35.7433	24.9746
7	238.7190	73.8922	7.1916	102.2304	67.1198	21.5920	37.8925	34.9793
8	243.3578	75.6878	4.2291	109.0616	64.9457	24.7774	36.4051	31.7485
9	235.1248	71.2926	5.9462	100.1200	61.0852	24.0519	38.5095	28.9500
10	236.8593	43.1350	3.9404	103.5211	48.2493	20.2185	37.6547	34.5452
11	249.1403	48.0462	3.1924	100.6876	56.9639	21.7398	39.6080	32.5651
12	242.8316	51.3860	6.6353	109.6458	50.1128	23.1082	39.0927	23.0888
13	241.7454	65.7497	5.1338	107.1166	68.7246	22.3311	35.5088	20.6045
14	233.4290	46.4425	4.5097	104.5962	54.0846	23.7993	38.9491	39.4324
15	240.0240	69.0459	7.7680	102.9260	63.5186	23.5377	36.8863	21.8074

Table 14 Numerical simulation results of responses for sampling points in Table 13

No.	Warpage [mm]	Minimum weldline temperature [°C]	Clamping force [tonne]	Cycle time [s]
1	18.98	232.1	6045.4	90.3573
2	14.71	235.4	6083.5	96.6877
3	13.87	245.5	6341.6	100.6981
4	11.21	229.9	6069.7	93.5495
5	12.62	247.7	6117.8	100.7357
6	13.13	244.8	5843.9	89.6254
7	12.47	238.3	5802.3	101.6554
8	14.97	242.7	6353.1	97.1600
9	16.47	234.3	5664.9	97.4576
10	17.96	236.4	5948.5	96.3589
11	19.69	248.5	5876.2	97.1053
12	10.78	242.2	6350.1	91.9251
13	15.75	241.1	6213.4	83.5783
14	16.18	232.9	5963.0	106.6904
15	12.27	239.3	5856.6	89.9995

References

1. Ozcelik B, Sonat I (2009) Warpage and structural analysis of thin shell plastic in the plastic injection molding. Mater Des 30(2):367–375
2. Oktem H, Erzurumlu T, Uzman I (2007) Application of Taguchi optimization technique in determining plastic injection molding process parameters for a thin-shell part. Mater Des 28(4):1271–1278
3. Tang SH, Tan YJ, Sapuan SM, Sulaiman S, Ismail N, Samin R (2007) The use of Taguchi method in the design of plastic injection mould for reducing warpage. J Mater Process Technol 182(1-3):418–426
4. Kurt M, Kamber OS, Kaynak Y, Atakok G, Girit O (2009) Experimental investigation of plastic injection molding: assessment of the effects of cavity pressure and mold temperature on the quality of the final products. Mater Des 30(8):3217–3224
5. Masato D, Rathore J, Sorgato M, Carmignato S, Lucchetta G (2017) Analysis of the shrinkage of injection-molded fiber-reinforced thin-wall parts. Mater Des 132:496–504
6. Wang Z, Zhang S, Qiu L, Liu X, Li H (2019) A low-carbon design method integrating structure design and injection process design for injection molding machines. Math Probl Eng 2019(11):1–19
7. Li C, Wang F, Chang Y, Liu Y (2010) A modified global optimization method based on surrogate model and its application in packing profile optimization of injection molding process. Int J Adv Manuf Technol 48(5-8):505–511
8. Gao YH, Wang XC (2009) Surrogate-based process optimization for reducing warpage in injection molding. J Mater Process Technol 209(3):1302–1309
9. Kitayama S, Yokoyama M, Takano M, Aiba S (2017) Multi-objective optimization of variable packing pressure profile and process parameters in plastic injection molding for minimizing warpage and cycle time. Int J Adv Manuf Technol 92(9-12):3991–3999
10. Hashimoto S, Kitayama S, Takano M, Kubo Y, Aiba S (2020) Simultaneous optimization of variable injection velocity profile and process parameters in plastic injection molding for minimizing weldline and cycle time. J Adv Mech Des Syst Manuf 14(3):JAMDSM0029
11. Ozcelik B, Erzurumlu T (2005) Determination of effecting dimensional parameters on warpage of thin shell plastic parts using integrated response surface method and genetic algorithm. Int Commun Heat Mass Transfer 32(8):1085–1094
12. Kurtaran H, Erzurumlu T (2006) Efficient warpage optimization of thin shell plastic parts using response surface methodology and genetic algorithm. Int J Adv Manuf Technol 27(5-6):468–472
13. Gao Y, Wang X (2008) An effective warpage optimization method in injection molding based on the Kriging model. Int J Adv Manuf Technol 37(9-10):953–960
14. Xia W, Luo B, Liao XP (2011) An enhanced optimization approach based on Gaussian process surrogate model for process control in injection molding. Int J Adv Manuf Technol 56(9-12):929–942
15. Chen W, Kurniawan D (2014) Process parameters optimization for multiple quality characteristics in plastic injection molding using Taguchi method, BPNN, GA, and Hybrid PSO-GA. Int J Precis Eng Manuf 15(8):1583–1593
16. Zhao J, Cheng G, Ruan S, Li Z (2015) Multi-objective optimization design of injection molding process parameters based on the improved efficient global optimization algorithm and non-dominated sorting-based genetic algorithm. Int J Adv Manuf Technol 78(9-12):1813–1826
17. Zhao J, Cheng G (2016) An innovative surrogate-based searching method for reducing warpage and cycle time in injection molding. Adv Polym Technol 35(3):288–297
18. Cheng J, Liu Z, Tan J (2013) Multiobjective optimization of injection molding parameters based on soft computing and variable complexity method. Int J Adv Manuf Technol 66(5-8):907–916
19. Liu J, Chen X, Lin Z, Diao S (2017) Multiobjective optimization of injection molding process parameters for the precision manufacturing of plastic optical lens. Math Probl Eng 2017:1–13
20. Xu G, Yang Z, Long G (2012) Multi-objective optimization of MIMO plastic injection molding process conditions based on particle swarm optimization. Int J Adv Manuf Technol 58(5-8):521–531
21. Xu G, Yang Z (2015) Multiobjective optimization of process parameters for plastic injection molding via soft computing and grey correction analysis. Int J Adv Manuf Technol 78(1-4):525–536
22. Dang XP (2014) General frameworks for optimization of plastic injection molding process parameters. Simul Model Pract Theory 41:15–27
23. Shi H, Xie S, Wang X (2013) A warpage optimization method for injection molding using artificial neural network with parametric sampling evaluation strategy. Int J Adv Manuf Technol 65(1-4):343–353
24. Deng YM, Zhang Y, Lam YC (2010) A hybrid of mode-pursuing sampling method and genetic algorithm for minimization of injection molding warpage. Mater Des 31(4):2118–2123
25. Dimla DE, Camilotto M, Miani F (2005) Design and optimisation of conformal cooling channels in injection moulding tools. J Mater Process Technol 164:1294–1300
26. Au KM, Yu KM (2007) A scaffolding architecture for conformal cooling design in rapid plastic injection moulding. Int J Adv Manuf Technol 34(5-6):496–515
27. Wang Y, Yu KM, Wang CC (2015) Spiral and conformal cooling in plastic injection molding. Comput Aided Des 63:1–11
28. Kitayama S, Yamazaki Y, Takano M, Aiba S (2018) Numerical and experimental investigation of process parameters optimization in plastic injection molding using multi-criteria decision making. Simul Model Pract Theory 85:95–105
29. Kitayama S, Tamada K, Takano M, Aiba S (2018) Numerical and experimental investigation on process parameters optimization in plastic injection molding for weldlines reduction and clamping force minimization. Int J Adv Manuf Technol 97(5-8):2087–2098
30. Kitayama S, Tamada K, Takano M, Aiba S (2018) Numerical optimization of process parameters in plastic injection molding for minimizing weldlines and clamping force using conformal cooling channel. J Manuf Process 32:782–790
31. Miettinen K (2014) Survey of methods to visualize alternatives in multiple criteria decision making problems. OR Spectr 36(1):3–37
32. Kim C, Wang S, Choi KK (2005) Efficient response surface modeling by using moving least-squares method and sensitivity. AIAA J 43(11):2404–2411
33. Lancaster P, Salkauskas K (1981) Surfaces generated by moving least squares methods. Math Comput 37(155):141–158
34. Deb K, Jain H (2013) An evolutionary many-objective optimization algorithm using reference-point-based nondominated sorting approach, Part I: solving problems with box constraints. IEEE Trans Evol Comput 18(4):577–601
35. Jain H, Deb K (2013) An evolutionary many-objective optimization algorithm using reference-point based nondominated sorting

approach, Part II: handling constraints and extending to an adaptive approach. IEEE Trans Evol Comput 18(4):602–622

36. Autodesk Moldflow Insight User's Guide, 2018. [Online]. Available: http:// https://knowledge.autodesk.com/support/moldflow-insight/learn-explore/caas/CloudHelp/cloudhelp/2018/ENU/MoldflowInsight/files/GUID-66B3B0E8-DB05-4DC5-8E8F-CCA29A11A7ED-htm.html. [Accessed 28 March 2017]